Geochemistry, Geophysics, Geosystems®

AGU ADVANCING EARTH AND SPACE SCIENCE

RESEARCH ARTICLE
10.1029/2021GC009986

The Lithophile Element Budget of Earth's Core

B. A. Chidester[1,2,3], S. J. Lock[4,5], K. E. Swadba[2], Z. Rahman[6], K. Righter[7], and A. J. Campbell[2]

[1]University of California Davis, Davis, CA, USA, [2]University of Chicago, Chicago, IL, USA, [3]Now at Los Alamos National Laboratory, Los Alamos, NM, USA, [4]California Institute of Technology, Pasadena, CA, USA, [5]University of Bristol, Bristol, UK, [6]Jacobs, NASA Johnson Space Center, Houston, TX, USA, [7]NASA Johnson Space Center, Houston, TX, USA

B. A. Chidester and S. J. Lock are co-first authors.

Key Points:

- We used new and previous data to constrain a thermodynamic model for metal-silicate partitioning
- Major lithophile-element partitioning can be used to constrain planet formation
- U could be significant for the thermal evolution of the core, but exsolution of oxides is likely not

Supporting Information:

Supporting Information may be found in the online version of this article.

Correspondence to:

B. A. Chidester,
bchides@lanl.gov

Citation:

Chidester, B. A., Lock, S. J., Swadba, K. E., Rahman, Z., Righter, K., & Campbell, A. J. (2022). The lithophile element budget of Earth's core. *Geochemistry, Geophysics, Geosystems*, *23*, e2021GC009986. https://doi.org/10.1029/2021GC009986

Received 17 JUN 2021
Accepted 26 JAN 2022

Author Contributions:

Conceptualization: B. A. Chidester, K. Righter, A. J. Campbell
Data curation: B. A. Chidester
Formal analysis: B. A. Chidester, K. E. Swadba
Funding acquisition: B. A. Chidester, K. Righter, A. J. Campbell
Investigation: B. A. Chidester, S. J. Lock
Methodology: B. A. Chidester, S. J. Lock, K. E. Swadba, Z. Rahman, A. J. Campbell
Software: S. J. Lock
Supervision: K. Righter, A. J. Campbell

Abstract The relative composition of Earth's core and mantle were set during core formation. By determining how elements partition between metal and silicate at high pressures and temperatures, measurements of the mantle composition and geophysical observations of the core can be used to understand the mechanisms by which Earth formed. Here we present the results of metal-silicate partitioning experiments for a range of nominally lithophile elements (Al, Ca, K, Mg, O, Si, Th, and U) and S to 85 GPa and up to 5400 K. With our results and a compilation of literature data, we developed a parameterization for partitioning that accounts for compositional dependencies in both the metal and silicate phases. Using this parameterization in a range of planetary growth models, we find that, in general, lithophile element partitioning into the metallic phase is enhanced at high temperatures. The relative abundances of FeO, SiO_2, and MgO in the mantle vary significantly between planetary growth models, and the mantle abundances of these elements can be used to provide important constraints on Earth's accretion. To match Earth's core mass and mantle composition, Earth's building blocks must have been enriched in Fe and depleted in Si compared with CI chondrites. Finally, too little Mg, Si, and O are partitioned into the core for precipitation of oxides to be a major source of energy for the geodynamo. In contrast, several ppb of U can be partitioned into the core at high temperatures, and this energy source must be accounted for in thermal evolution models.

Plain Language Summary As a planet grows, it becomes hot enough to melt and separate into a metallic core and a rocky mantle. During this process, elements are exchanged between the rock and the metal at temperatures of thousands of degrees and pressures hundreds of thousands of times greater Earth's atmosphere. This chemical exchange sets the compositions of the core and mantle. To improve our understanding of core formation, we conducted experiments examining how different elements exchange between molten metal and molten rock at the pressures and temperatures of planet formation. Using our data and a collection of data from other experiments, we have built a tool that can predict how elements will behave at different conditions. We find that elements that normally stay totally in the rock at moderate temperatures and pressures start moving into the metal at the very high pressures and temperatures of core formation. By looking at the abundance of those elements in the rocky part of Earth today, we may be able to work out what material the Earth formed from and under what pressures and temperatures core formation occurred. Our results also give us insight into how Earth's magnetic field has been powered for billions of years.

1. Introduction

The chemical compositions of the cores and mantles of the terrestrial planets are mostly set during equilibration between iron-rich metal and silicate material as the planets grow. The growth process is stochastic and the details of how, and under what conditions, equilibration occurs are uncertain. Due to the large volume of data available, the Earth can serve as a proving ground for models of terrestrial core formation. How different elements partition between metal and silicate, and so how elements are divided between the mantle and core, depends on the pressure and temperature of equilibration, as well as the composition of the equilibrating system. The compositions of the mantle and core of Earth therefore provide a record of the accretional history of the planet. Any model of Earth's core formation should match the mantle composition of the major and trace elements (e.g., Fischer et al., 2018; Piet et al., 2017; Rubie et al., 2011; Rudge et al., 2010; Wade & Wood, 2001). Traditionally, the moderately siderophile elements (e.g., Ni, Co, V, and Cr), those that have somewhat similar preferences for both the metal and silicate, have been used as the principal constraint on the accretional history of Earth (e.g., Fischer et al., 2015; Siebert et al., 2012). However, recent studies have shown that nominally lithophile elements, those that preferentially partition into silicates under ambient conditions, can be affected by the core formation process

Writing – original draft: B. A. Chidester, S. J. Lock
Writing – review & editing: B. A. Chidester, S. J. Lock, K. E. Swadba, K. Righter, A. J. Campbell

when equilibration occurs at very high pressure-temperature (*P-T*) conditions (e.g., Badro et al., 2016; Blanchard et al., 2017; Chidester et al., 2017; Faure et al., 2020; Wade & Wood, 2001; Wohlers & Wood, 2015, 2017). The strongly lithophile elements have the potential to be hallmarks of the most extreme equilibration conditions during planet formation, but more work is needed to understand their partitioning behavior at the high pressure and temperature conditions of core formation.

The composition of Earth's core controls the dynamics within the planet. For example, Earth's magnetic field today is largely driven by elemental partitioning between the solidifying inner core and the liquid outer core, and possibly in the past by radioactive decay or precipitation of low-density oxide materials at the core-mantle boundary (CMB) as the core cooled from its initially hot state (e.g., Hirose et al., 2017; Nimmo, 2015a; O'Rourke & Stevenson, 2016; O'Rourke et al., 2017). One major constraint on the core's energy budget is that sufficient dissipative entropy must have been produced to generate the geomagnetic field for at least the last 3.5 Gyr (Nimmo, 2015a; Tarduno et al., 2010), and possibly much longer (Tarduno et al., 2015). Core evolution models that only include secular cooling and the energy provided by inner-core growth imply that the initial temperature at the CMB would have been high enough that the lowermost, and potentially the whole, mantle would have been substantially molten through much of Earth's history (Nimmo, 2015a). An additional energy source is required to reconcile such thermal evolution models and observations.

If sufficient radioactive elements are present in the core, heat produced by their decay would have allowed the core to cool more slowly while maintaining a magnetic field, such that the modeled CMB temperatures early in Earth's history are more reasonable. According to recent thermal evolution models, adding the equivalent of 200–400 ppm K to the core (minimum of 1.4 TW of heat production today, 17 TW of heat at 4.568 Gyr) and assuming a relatively low thermal conductivity of core material (50 W/mK), the initial CMB temperature could have been low enough to be consistent with observations of solid-state mantle flow and inner core size (Nimmo, 2015a; Nimmo et al., 2004). Recent metal-silicate partitioning studies of U and K at the relevant conditions of core formation indicate that it is unlikely that these elements were incorporated into the core in sufficient quantities to greatly affect core cooling (Blanchard et al., 2017; Chidester et al., 2017; Faure et al., 2020). However, these studies have also shown that lithophile elements partition differently at the extreme pressures and temperatures of core formation than had been expected, and more experiments are required to fully quantify partitioning at all relevant conditions. Additionally, the metal-silicate partitioning of Th, which is 4 times more abundant than U at present day, has not been thoroughly explored.

Another proposed solution to the core energy budget is the possibility that high concentrations of major elements (Mg, Si, and O) dissolved into the core during the extreme pressure and temperature events of planetary accretion and then were subsequently precipitated at the CMB as the core cooled (Badro et al., 2016; Hirose et al., 2017; O'Rourke & Stevenson, 2016; O'Rourke et al., 2017). Precipitation of MgO and SiO_2, and the associated sinking of the denser residual iron-rich material, could release more gravitational potential energy than is derived from the growth of the inner core, potentially providing sufficient energy to drive the geodynamo for much of Earth's history without having to invoke high initial CMB temperatures (O'Rourke & Stevenson, 2016). This hypothesis requires that the partitioning of major elements into the core is strongly enhanced at high temperature and not suppressed at the high pressures of the CMB, which is debated (Badro et al., 2016, 2018; Du et al., 2017; Hirose et al., 2017; Mittal et al., 2020) partly due to the sparsity of data.

It is clear that more data on the partitioning of nominally lithophile elements is needed to be able to place constraints on the accretion of Earth and to determine what mechanisms could be responsible for the longevity of the geodynamo. Here we present new metal-silicate partitioning measurements between 1 and 85 GPa and up to 5400 K for a range of nominally lithophile, and major light elements, including Al, Ca, K, Mg, O, S, Si, Th, and U. We then use our data, combined with a collection of previous studies, to constrain the chemical behavior of these elements under a wide range of pressure, temperature, and compositional conditions. Our results are fundamentally different than those inferred in previous metal-silicate partitioning studies, particularly in terms of the effect of silicate melt structure and composition on partitioning. We use our partitioning relations within simple planetary growth models to explore the range of possible terrestrial core and mantle compositions. We then discuss the implications of our results for the composition of the mantle and core and the energy budget of the core.

2. Experimental Methods

2.1. High-Pressure, High-Temperature Partitioning Experiments

Metal-silicate partitioning experiments of lithophile elements were completed in a laser-heated diamond anvil cell (LH-DAC) between 23 and 85 GPa in the Laboratory for Mineral Physics at the University of Chicago. The results for several of the U-containing samples in this study (B49, B66) were reported previously, and many of the methods used here are identical (Chidester et al., 2017).

The silicate material used in most experiments was a mixture of oxides of approximately pyrolite major-element composition (McDonough & Sun, 1995), except containing no initial FeO to promote reducing conditions relevant to planet formation. To facilitate analytical measurement of the radioactive elements, U, Th, and K, these elements were enriched in the silicate material with respect to their natural abundances. The starting compositions for each sample are listed in Table S1 of Supporting Information S2. MgO (99%), Al_2O_3 (99.99%), SiO_2 (99.9%), $CaSiO_3$ (meta, reagent grade), SiO_2:K_2O (2.5:1 by weight, 48 mesh), Fe (99.9+%, <10 μm), FeSi (99.9%) and FeS (99.9%) were all purchased from Alfa Aesar. The oxide and silicate powders were fired in a furnace at 1100°C for 12–20 hr to remove any contaminating OH prior to use. ThO_2 (99.99%) was purchased from Strem Chemical and was not processed further. Depleted UO_2 powder was purchased from SPI Chemical; this material contained a small amount of polymer binder, so it was washed in ethanol and dried at 100°C prior to sample preparation. To promote homogeneity, the silicate mixtures were ball-milled in a tungsten carbide capsule at 20 Hz for 1.5 hr.

The metal used in these experiments was either stoichiometric FeSi, Fe–9Si (i.e., an alloy with 9 weight percent Si), or a mixture of FeSi, FeS, and Fe, to produce Fe alloys of varying compositions during the experiment. The metals were also blended in a tungsten carbide capsule using a ball mill at 20 Hz for 1.5 hr. Tungsten was not detected in any of the samples; however, it is possible that trace W was introduced during the ball milling processes and that it was not observed as a result of a strong peak overlap between W and Si using energy dispersive analytical techniques.

Due to the extremely small scale of the samples in diamond anvil cell experiments, neither the proportions of metal and silicate in the starting material nor the oxygen fugacity ($f\,O_2$) can be precisely controlled *a priori*. The oxygen fugacity was self-imposed by the exchange of Fe and Si between the metal and silicate melts at high *P-T* conditions. We attempted to influence this reaction by keeping FeO contents in the silicate starting material low and increasing the amounts of Si in the starting metal, but the chemistry at these high *P-T* conditions typically drives the oxygen fugacity to a narrow range of ΔIW, as noted previously (Badro et al., 2016; Chidester et al., 2017; Du et al., 2017; Fischer et al., 2015; Siebert et al., 2012, 2018; Suer et al., 2017). In our experiments, $f\,O_2$ is determined by comparing the coexisting metal and silicate products after sample recovery. Details of that calculation are given below. Importantly, the oxygen fugacity that was established during the experiment is relevant to high-pressure core formation conditions (Rubie et al., 2011).

Diamond anvil cell samples were loaded into stainless steel gaskets pre-indented to 18–23 GPa or rhenium gaskets pre-indented to 25–28 GPa. The diamond culets measured 300, 250, or 150 μm in diameter. The metallic sample material was pressed into a thin foil of 2–5 μm thick and encapsulated within the sample chamber between flakes of silicate powder. The samples were dried at 90°C for 30–60 min after loading but prior to closing the cell to remove any adsorbed moisture from the sample. Prior to heating, the pressure at the location to be heated was determined using the Raman shift of diamond (calibrated to ruby under quasi-hydrostatic conditions after Akahama and Kawamura [2007]). The comparison of several measurements across the sample chamber confirmed that the stress state in the sample chamber was relatively hydrostatic within 1–2 GPa. Any non-hydrostatic strain within the sample is expected to be alleviated upon melting of the sample. Thermal pressure was estimated assuming a linear dependence on temperature of $\Delta P = 2.7$ MPa/K from Siebert et al. (2012). This is different from the thermal pressure estimate reported previously, where ΔP was taken to be 20% of the room temperature pressure (Chidester et al., 2017). The difference between these pressure estimates was at most a few GPa. Samples were heated using a double-sided version of the laser-heating system described in Campbell (2008). Laser-heating was accomplished by gradually increasing the laser power to above the sample liquidus over a period of ∼5 min. The samples were held at the peak temperature for 30–60 s, and then samples were quenched to room temperature by cutting power to the laser. Surface temperatures were measured spectro-radiometrically (Heinz

& Jeanloz, 1987). The axial temperature gradient across the metal foil was then accounted for by correcting the surface temperature by −3%, as recommended by Campbell et al. (2007).

Samples were recovered using a dual beam focused ion beam (FIB/SEM) at either Johnson Space Center (FEI Quanta 3D FEG) or the University of Chicago (Tescan Lyra3). Samples were sectioned along the axis of compression through the laser heated spot, attached to a copper TEM grid with a Pt strip and thinned to ∼1 μm. The TEM grid was adhered to a copper SEM stub for chemical analysis, rather than an Al one, so that measurements of Al would include as little contamination from the system as possible.

Additionally, a set of four new piston-cylinder experiments was completed with varying UO_2 contents to explicitly assess the partitioning of U as a function of UO_2 in the silicate melt. The starting compositions for these experiments are also listed in Table S1 of Supporting Information S2, where the metal and silicate phases were initially combined 50/50 by weight and homogenized in a tungsten carbide capsule in a ball mill. Samples, contained in graphite capsules, were compressed to 1 GPa and heated to 2173 K in a non-end-loaded piston-cylinder apparatus at NASA-Johnson Space Center. The runs were brought to temperature over 55 min, then allowed to equilibrate for 10 min. Temperatures were measured with a W5Re/W25Re thermocouple. Samples were thermally quenched by cutting power to the furnace. More complete experimental details can be found elsewhere (Filiberto et al., 2008; Righter et al., 2006).

2.2. Chemical Analysis

Chemical analyses were carried out using energy dispersive X-ray spectroscopy (EDX) on a Tescan Lyra3 scanning electron microscope (SEM) at 15 kV. The electrical current on this system was adjusted to maximize counts to the EDX detector but was always less than 2 nA. Profiles were taken in 20 nm steps with 10 ms dwell time per pixel. Compositions were determined by averaging all the point measurements from each phase. As such, the measurements reported are very precise, while their analytical accuracy is estimated to be better than 10% (relative) based on analytical standards. Details on the analytical accuracy of the EDX system are available in Table S2 of Supporting Information S2 and discussed in Supporting Information S1. In cases where the silicate melt region was radially small compared with the activation volume of the EDX measurements, the compositions of those phases were determined by fitting with a point-spread function as described by Chidester et al. (2017).

The samples in this study were thinned to ∼1 μm, which is typically less than the probe depth of the EDX measurement. This is essential for measurements of recovered DAC samples due to their very small scale and high probability of obtaining signal from material outside the melted region. Because the samples are thinner than typical standards, analyses were normalized to 100 mol %. It has been suggested that thin samples will show a systematic dependence on the thickness of the sample when the samples are thinner than the standards (Jennings et al., 2019). We tested whether this would be an issue when normalizing to 100% and find that there is no difference in natural olivine compositions when the sample is between 0.8 and 3.3 μm thick (see Figure S1 and discussion in Supporting Information S1 for details). Additionally, oxide mole fractions were determined assuming standard oxidation states for the cations in the silicate melt, with the exception of U, which was inferred to be in the 2+ oxidation state (Blanchard et al., 2017; Chidester et al., 2017), and S, which was assumed to have an oxidation state of 0 (see below). An example back-scattered electron image of a recovered DAC sample is given in Figure 1a. EDX measurements on samples B49 and B66, which were reported previously (Chidester et al., 2017), were reanalyzed on a Cu SEM stub to increase confidence in the Al measurements. We were unable to reanalyze samples B42, B50, and B56 from Chidester et al. (2017), so they are not used in the analysis reported here. Additionally, samples B22 and B23 represent extreme end-member compositions that are not representative of Earth's mantle, so they are also excluded from the analysis described below (Chidester et al., 2017).

Piston-cylinder (PC) samples were chemically analyzed using both EDX at the University of Chicago (major elements) and laser ablation inductively coupled plasma mass spectrometry (LA-ICP-MS) at the University of Houston (trace elements). An example back-scattered electron image of one of the recovered piston-cylinder samples is shown in Figure 1b. EDX measurements of these samples were averaged over several boxes of differing dimensions to account for the quench texture (Figure 1b inset). All other EDX settings were the same as the recovered DAC samples described above. LA-ICP-MS measurements were made using a Photon Machines Inc. Analyte.193 ArF laser ablation system coupled to a Varian 810-MS ICP-MS. The laser operated with a repetition rate of 4–19 Hz at 3 J/cm^2 and a helium flow rate of 0.5 L/min. The spot sizes were 50–100 μm. Background

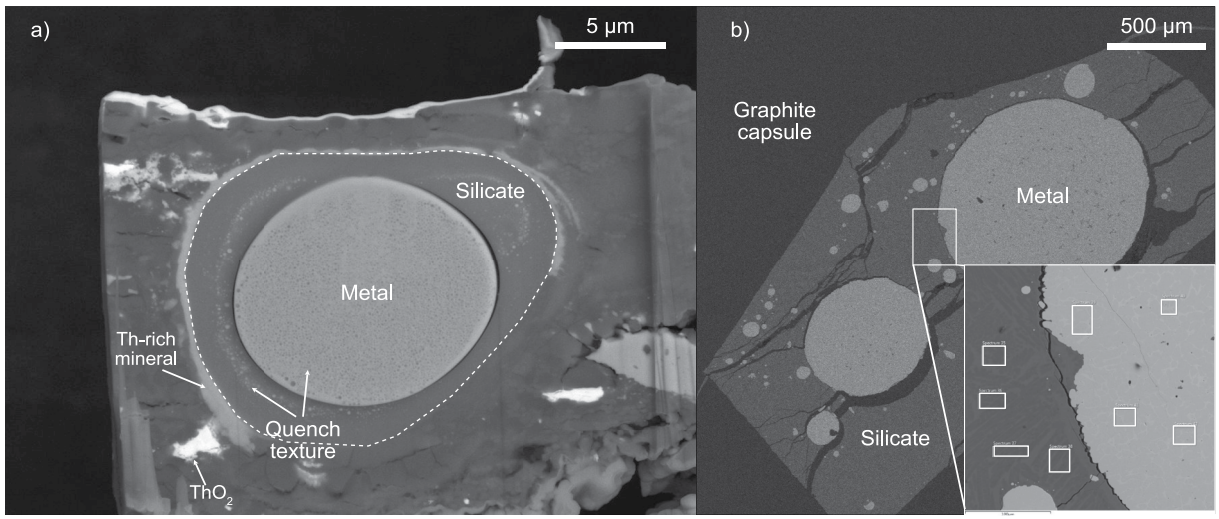

Figure 1. Example back-scattered electron images of metal-silicate partitioning samples. (a) Sample B85, recovered from 41 GPa to 3400 K. The central bright region is the metal, which is surrounded by silicate glass. There is a bright Th-rich band outside of the silicate glass. The melt region is denoted by a dashed line. (b) Sample PC0p4, recovered from 1 GPa to 2173 K. Inset shows a zoomed in portion showing regions of chemical analysis in white boxes.

measurements were made over 20 s, then ablation proceeded for 30 s, and the final washout occurred over 20 s, for a total of 70 s per measurement. The isotopes measured in both the silicate and metal melts in each sample were: ^{29}Si, ^{43}Ca, ^{49}Ti, ^{56}Fe, ^{61}Ni, ^{60}Ni, ^{232}Th, and ^{238}U. Three separate measurements were made in each phase and averaged to produce the final concentration. The measurements were calibrated using NIST 610 and NIST 612 glass standards (Pearce et al., 1997) and the data were reduced using the Glitter software package (van Achterbergh et al., 1999).

Notably, we do not report the C contents of our PC samples, despite the probability of C contamination from the graphite capsules. It is difficult to measure the C contents of recovered metals with any degree of certainty because C is a ubiquitous contaminant (see Fischer et al. [2015] for example). Righter et al. (2010) showed that melting experiments in graphite capsules can result in metals with up to 6 wt% C. However, our PC experiments were conducted with FeSi liquids, and Si and C have been shown to be inversely correlated in metallic liquids (Lacaze & Sundman, 1991; Vander Kaaden et al., 2020). Based on those results, we expect our PC samples to contain <0.5 wt% C. Additionally, our PC experiments were devised to measure the effect of the UO_2 abundance on U partitioning. The Steelmaking Data Sourcebook (Japan Society for the Advancement of Science and the 19th Committee on Steelmaking, 1988) gives the interaction parameters between U and C as 0 in metallic melts, and other metal-silicate experiments on U conducted in both graphite and MgO capsules has shown no significant difference based on capsule material (Bouhifd et al., 2013). Thus, given the high Si contents of the metals in our study, and the negligible interaction between U and C, we expect our parameterization to be accurate without including a parameter for the C content. Since C is such a difficult element to measure and has been inconsistently reported in the literature, we do not include C in our parameterization.

3. Results

3.1. Textural Analysis and Equilibrium

In total, nine metal-silicate partitioning experiments were completed in a LH-DAC between 23 and 85 GPa, including several reanalyzes from Chidester et al. (2017), and four metal-silicate partitioning experiments were conducted in a piston-cylinder apparatus at 1 GPa and 2173 K. The conditions (P, T, and fO_2) of the experiments from this study are listed in Table 1, and the metal and silicate melt compositions of the recovered samples are listed in Tables S3 and S4 of Supporting Information S2, respectively. The oxygen fugacity (fO_2) of each experiment listed in Table 1 is calculated in reference to the iron-wüstite buffer:

$$\Delta IW = -2 \times log_{10}\left(\frac{a_{Fe}}{a_{FeO}}\right) = -2 \times log_{10}\left(\frac{\gamma_{Fe}x_{Fe}}{\gamma_{FeO}x_{FeO}}\right), \quad (1)$$

Table 1
Experimental Conditions for the Metal-Silicate Partitioning Experiments in This Study

Sample	P_0 (GPa)	P (GPa)	T (K)	T error (K)	fO_2 (ΔIW)
B59	16	23	3213	249	−1.72
B64	29	39	3895	227	−1.57
B72	40	50	4163	174	−2.45
B77	46	58	4790	184	−2.26
B83	74	85	4495	473	−1.63
B85	33	41	3417	325	−2.04
B91	52	64	4696	236	−1.50
PC0p1	-	1	2173	100	-
PC0p4	-	1	2173	100	−4.73
PC2	-	1	2173	100	−5.98
PC12	-	1	2173	100	−4.54
B49[a]	47	60	5354	257	−1.55
B66[a]	46	57	4380	264	−2.20

[a]Sample reanalyzed from Chidester et al. (2017).

"P_0" is the room-temperature pressure measured prior to heating, P is the pressure at the temperature of the experiment estimated by taking the room-temperature P and adding the thermal pressure assuming $\Delta P = 2.7$ MPa/K (Siebert et al., 2012). The error on pressure is estimated to be 10% of the high-temperature pressure. fO_2 was calculated using Equation 1 with the activity of FeO equal to its mole fraction. For sample PC0p1 the fO_2 could not be determined as both the amount of O in the metal and FeO in the silicate were below their respective detection limits.

where γ_{Fe} is the activity coefficient of iron in the metal, γ_{FeO} is the activity coefficient of FeO in the silicate, x_{Fe} is the measured molar fraction of iron in the metal, and x_{FeO} is the measured molar fraction of FeO in the silicate. Here we have determined the activity coefficients, γ_i, using the thermodynamic parameterization described in Section 3.3. Whereas γ_{Fe} calculated using our parameterizations is always close to unity, γ_{FeO} is typically substantially greater than unity (~3–5), which results in calculated oxygen fugacities that are likely unrealistically oxidized (see discussion below). This is not surprising given the simplicity of our silicate melt activity model and so we take $\gamma_{FeO} = 1$ (i.e., the activity is equal to the mole fraction FeO) when calculating the fO_2 reported in Table 1.

The recovered samples all exhibited a texture similar to those from previous experiments (Badro et al., 2016; Blanchard et al., 2017; Chidester et al., 2017; Du et al., 2017; Fischer et al., 2015; Jackson et al., 2018; Siebert et al., 2012); a coalesced metal ball surrounded by silicate glass (Figure 1). This texture is ubiquitously observed when the sample has been subjected to temperatures above the liquidi of both metal and silicate. This observation and the flat compositional profiles across regions of the sample with different length scales serve as evidence of local chemical equilibrium at the experimental conditions.

In the DAC samples, a small scale, spatially homogeneous quench texture was often observed within the metallic region and a heterogeneous quench texture with Fe-rich blebs was often observed in the silicate melt, reflecting the difference in quench rates across the silicate (Figure 1a). Indeed, the exsolved blebs in the silicate melt are localized away from the rim of the heated spot where quench rates would have been much quicker as that region is closer to the diamonds. The bulk silicate melt composition was the same within error regardless of whether the analyses were averaged over a homogeneous or heterogeneous region, suggesting that the Fe-rich blebs in the silicate melt were exsolved on quench rather than incompletely incorporated into the metal ball. Still, analyses in the heterogeneous regions were avoided whenever possible.

All experiments containing Th had a Ca- and Th-rich silicate mineral just outside of the melt region (e.g., Figure 1). Although the spatial resolution of our measurements was not high enough for us to ascertain the stoichiometry of this mineral, it is likely Ca-perovskite or an unknown accessory phase. While Ca-perovskite is not expected to be the liquidus phase at these pressures (e.g., Ito et al., 2004; Trønnes et al., 2019), the presence of Th can increase the entropy of this mineral, stabilizing it at higher temperatures. Interestingly, both Th and U are an incompatible elements at lower pressures, so Th is expected to partition into the liquid. U remains incompatible over the whole range of pressures studied (23–67 GPa) and is never concentrated in the solid phase, even though this phase is observed in all Th bearing samples in this study (41–85 GPa) and two samples in Chidester et al. (2017) that contained both U and Th. This suggests a change in the mineral compatibility of Th and a fractionation between U and Th at conditions above at least 40 GPa which could have profound implications for the radiogenic heat budget of Earth's mantle. While we do not have a satisfactory reason why Th should become more compatible at high pressures, one possible reason for the difference in U and Th behavior is that U could be stabilized in the melt in the 2+ oxidation state, as has been suggested previously (Chidester et al., 2017). A change in oxidation state would change the physical size of the cations, affecting their compatibility within melts and minerals (e.g., Blundy & Wood, 1994).

The piston-cylinder samples also exhibited a quench texture (Figure 1b). The BSE image shows darker and lighter regions within the metal, suggesting higher and lower Si concentrations, respectively. The silicate primarily quenched to a glass, but we do observe some crystallite spindles. In our analyses, we accounted for the heterogeneous silicate quench texture by averaging the compositions measured over swaths of the sample rather than discrete points (see boxes in Figure 1b inset).

3.2. Exchange Coefficients

Using our experimental results we can determine the strength of partitioning of different elements between metal and silicate at the probed thermodynamic conditions. Metal-silicate partitioning is usually quantified using exchange coefficients, the definition of which depends on the reaction that is assumed to be controlling partitioning of the element. The most common reaction used to describe metal-silicate partitioning is the redox exchange reaction

$$\mathrm{MO}_{n/2} + \frac{n}{2}\mathrm{Fe} \rightleftharpoons \mathrm{M} + \frac{n}{2}\mathrm{FeO}, \tag{2}$$

where an element M of valence n is either reduced by Fe or oxidized by FeO to be transferred between the metal and silicate. In this case, the exchange coefficient for partitioning of element M can be written

$$\begin{aligned}\log_{10} K_D^M &= \log_{10} \frac{x_{M,\mathrm{met}} \; x_{\mathrm{FeO,sil}}^{n/2}}{x_{MO_{n/2},\mathrm{sil}} \; x_{\mathrm{Fe,met}}^{n/2}} \\ &= a_M + \frac{b_M}{T} + c_M \frac{P}{T} + \frac{n}{2}\log_{10}\gamma_{\mathrm{Fe,met}} + \log_{10}\gamma_{MO_{n/2},\mathrm{sil}} \\ &\quad - \log_{10}\gamma_{M,\mathrm{met}} - \frac{n}{2}\log_{10}\gamma_{\mathrm{FeO,sil}}.\end{aligned} \tag{3}$$

where $x_{i,p}$ is the molar fraction and $\gamma_{i,p}$ is the activity coefficient, respectively, of element (or oxide) i in phase p (either metal or silicate). The coefficients, a_M, b_M, and c_M are the change in entropy, enthalpy, and volume, respectively, for the reaction in Equation 2. Note that for elements which exist in the atomic state in the silicate melt (i.e., $n = 0$), the exchange coefficient reduces to a partition coefficient, $D = x_{M,met}/x_{M,sil}$.

Alternatively, metal-silicate partitioning can be expressed as a dissociation reaction

$$\mathrm{MO}_{n/2} \rightleftharpoons \mathrm{M} + \frac{n}{2}\mathrm{O}, \tag{4}$$

in which case

$$\begin{aligned}\log_{10} K_D^M &= \log_{10} \frac{x_{M,\mathrm{met}} \; x_{\mathrm{O,met}}^{n/2}}{x_{MO_{n/2},\mathrm{sil}}} \\ &= a_M + \frac{b_M}{T} + c_M \frac{p}{T} - \frac{n}{2}\log_{10}\gamma_{\mathrm{O,met}} + \log_{10}\gamma_{MO_{n/2},\mathrm{sil}} - \log_{10}\gamma_{M,\mathrm{met}}.\end{aligned} \tag{5}$$

In particular, it has been suggested that the partitioning of Mg could be more accurately described by a dissociation reaction rather than an exchange reaction (Badro et al., 2018) and we will discuss this point later in the paper.

As O is an anion, its partitioning is inextricably linked to Fe and so must be treated differently to other elements. The partitioning of oxygen between metal and silicate is calculated by modeling partitioning as a dissociation reaction for wüstite, FeO.

$$\mathrm{FeO} \rightleftharpoons \mathrm{Fe} + \mathrm{O}, \tag{6}$$

in which case

$$\begin{aligned}\log_{10} K_D^{\mathrm{O}} &= \log_{10} \frac{x_{\mathrm{O,met}} \; x_{\mathrm{Fe,met}}}{x_{FeO,\mathrm{sil}}} \\ &= a_{\mathrm{O}} + \frac{b_{\mathrm{O}}}{T} + c_{\mathrm{O}} \frac{p}{T} - \log_{10}\gamma_{\mathrm{O,met}} + \log_{10}\gamma_{FeO,\mathrm{sil}} - \log_{10}\gamma_{\mathrm{Fe,met}}.\end{aligned} \tag{7}$$

The experimentally determined K_D^M for the samples in this study, assuming that all elements except for oxygen partition via an exchange reaction as described by the first lines of Equations 3 and 7, are listed in Table 2.

3.3. Parameterization of Metal-Silicate Partitioning

The raw chemical data from this study and an extensive compilation of the literature (Badro et al., 2016, 2018; Blanchard et al., 2017; Bouhifd & Jephcoat, 2003, 2011; Bouhifd et al., 2007, 2013; Boujibar et al., 2014, 2019;

Table 2
Exchange Coefficients for All Elements and Samples in This Study

Sample	$log_{10}K_D^{Al}$	$log_{10}K_D^{Ca}$	$log_{10}K_D^{K}$	$log_{10}K_D^{Mg}$	$log_{10}K_D^{O}$	$log_{10}K_D^{S}$	$log_{10}K_D^{Si}$	$log_{10}K_D^{Th}$	$log_{10}K_D^{U}$
B59	bdl	bdl	-	bdl	$-0.25^{+0.10}_{-0.11}$	-	$-2.00^{+0.09}_{-0.10}$	-	bdl
B64	$-2.8^{+0.2}_{-0.4}$	bdl	-	$-2.52^{+0.15}_{-0.20}$	$-0.13^{+0.07}_{-0.07}$	$0.49^{+0.04}_{-0.04}$	$-2.35^{+0.09}_{-0.09}$	-	$-2.01^{+0.16}_{-0.23}$
B72	$-3.15^{+0.12}_{-0.14}$	bdl	$-2.5^{+0.2}_{-0.3}$	$-2.8^{+0.09}_{-0.09}$	$0.49^{+0.08}_{-0.07}$	-	$-2.90^{+0.13}_{-0.16}$	$-4.0^{+0.3}_{-0.4}$	-
B77	$-3.1^{+0.2}_{-0.3}$	bdl	$-2.1^{+0.2}_{-0.3}$	$-2.50^{+0.18}_{-0.25}$	$0.19^{+0.14}_{-0.15}$	$0.96^{+0.09}_{-0.08}$	$-3.0^{+0.2}_{-0.3}$	bdl	-
B83	$-2.29^{+0.13}_{-0.15}$	$-2.1^{+0.2}_{-0.3}$	$-1.79^{+0.12}_{-0.15}$	$-2.03^{+0.12}_{-0.13}$	$0.12^{+0.09}_{-0.08}$	$0.99^{+0.10}_{-0.09}$	$-1.86^{+0.14}_{-0.16}$	$-2.60^{+0.19}_{-0.22}$	-
B85	$-3.1^{+0.2}_{-0.4}$	bdl	bdl	bdl	$-0.08^{+0.06}_{-0.06}$	-	$-2.51^{+0.09}_{-0.10}$	bdl	-
B91	$-2.28^{+0.17}_{-0.20}$	bdl	bdl	$-2.25^{+0.18}_{-0.25}$	$-0.03^{+0.10}_{-0.08}$	-	$-1.54^{+0.17}_{-0.20}$	bdl	-
PC0p1[a]	bdl	bdl	-	bdl	Bdl	-	$0.045^{+0.010}_{-0.010}$	-	$-1.35^{+0.03}_{-0.03}$
PC0p4	bdl	bdl	-	bdl	Bdl	-	$-4.7^{+0.2}_{-0.3}$	-	$-3.87^{+0.12}_{-0.15}$
PC2	bdl	bdl	-	bdl	Bdl	-	$-6.0^{+0.3}_{-0.4}$	-	$-4.73^{+0.13}_{-0.18}$
PC12	bdl	bdl	-	bdl	Bdl	-	$-4.51^{+0.14}_{-0.17}$	-	$-3.62^{+0.09}_{-0.09}$
B49[b]	$-2.19^{+0.07}_{-0.07}$	bdl	-	$-1.91^{+0.05}_{-0.05}$	$0.09^{+0.04}_{-0.04}$	$0.61^{+0.03}_{-0.03}$	$-1.76^{+0.07}_{-0.08}$	-	$-0.94^{+0.04}_{-0.05}$
B66[b]	$-3.08^{+0.15}_{-0.19}$	bdl	-	$-2.68^{+0.10}_{-0.12}$	$0.35^{+0.06}_{-0.05}$	$0.26^{+0.03}_{-0.03}$	$-2.76^{+0.10}_{-0.12}$	-	$-1.70^{+0.07}_{-0.07}$

Note. To correctly describe the non-symmetric error distribution on the partitioning coefficients derived from experimental measurement of the concentrations in the metal and silicate phase, we used a Monte-Carlo (MC) scheme with 100,000 draws to sample the error in the experimentally determined concentrations. We report the median of the $log_{10}K_D$ calculated from the MC points as the value for $log_{10}K_D$ (this is generally very similar to the $log_{10}K_D$ calculated from the raw experimental data) and the 16th and 84th percentiles as the 1–σ error envelope. A dash means the element was not present in the sample and "bdl" means the element was present but was below the detection limit of the instrument.

[a]Sample FeO was below the detection limit and hence $log_{10}D$ is reported instead of $log_{10}K_D$. [b]Sample reanalyzed from Chidester et al. (2017).

Chidester et al., 2017; Corgne et al., 2007; Du et al., 2017; Faure et al., 2020; Fischer et al., 2015; Jackson et al., 2018; Malavergne et al., 2007; Suer et al., 2017; Wade & Wood, 2001, see Table S5 in Supporting Information S2) were combined to develop a parameterization for metal-silicate partitioning of Al, Ca, K, Mg, O, S, Si, Th, and U, over a wide range of temperatures, pressures and compositions. Our compilation includes 196 individual samples, giving 674 individual measured K_D^M. This is not a complete list of all metal-silicate partitioning studies that have been conducted, but we have restricted our data compilation to studies that focus on lithophile element partitioning. Not all literature samples were treated in the same way as in this study; in particular, not all samples were thinned to thicknesses less than the probe depth to ensure there was no contamination of the signal in EDX measurements from outside the melted region. For consistency, all literature values for fO_2, partition, and exchange coefficients used in this study have been recalculated from the reported raw chemical data. We also examined all available sample images to ensure that the experiments used in our parameterization are probing equilibrium liquid metal-liquid silicate partitioning.

A full description of our metal-silicate partitioning parameterization is given in Supporting Information S1 but here we provide a brief summary. To calculate partitioning, we require models of the activity of each element in both the metal and silicate phases (e.g., Equations 3, 5, and 7). We derive the activity coefficients for elements in the metal using the standard ε-formulation of Ma (2001). For the activity of oxides in the silicate melt, we use a simple Margules-type multicomponent regular solution model (e.g., Mukhopadhyay et al., 1993). This is the first time such a model has been used in a metal-silicate partitioning parameterization. Many previous studies use a term dependent on the "non-bridging oxygens per tetrahedron" (nbo/t) to describe the effect of the structure of the silicate melt on partitioning. However, this parameter is only valid in low-pressure experiments below the transition of silicate tetrahedra to octahedra at mid-mantle pressures, which makes it a sub-optimal parameter when comparing low- and high-pressure data. Other studies have held that the silicate melt composition has little effect on the metal-silicate partitioning of moderately siderophile elements, such as Ni and Co in the 2+ valence (Blanchard et al., 2017; Fischer et al., 2015; Siebert et al., 2011; Wade & Wood, 2005). This can be

traced back to one study (O'Neill & Eggins, 2002) that suggested that the ratio of oxide activity coefficients in Equation 3 is insensitive to the silicate melt composition. However, large and sometimes high-charge cations may be more strongly affected by the silicate melt composition, so we make it a point to include the excess Gibbs free energy of the silicate melt in our fits (Equation S20 in Supporting Information S1).

In including a more complex silicate activity model in our parameterization we are not aiming to provide a complete description of the thermodynamics of the silicate melt. Recent attempts to produce thermodynamic models for the MgO-FeO-SiO_2 system (Boukaré et al., 2015; Miyazaki & Korenaga, 2019) show significant disagreements in key parameters and the currently available experimental data is not sufficient to produce an accurate description of the activity of many of the elements considered in this study. A more complete treatment would likely require, for example, pressure and temperature dependencies on the Margules parameters. Rather, by including a silicate activity model, we aim to have a framework which will allow us to examine the potentially complex dependence of metal-silicate partitioning on the melt composition and structure. Activity models of silicate melts will likely continue to improve with additional experimental data, and we plan to include a more complete and accurate model of silicate activity in future work.

We performed a linear least squares fit to determine the best-fit values, errors and correlations of the parameters that describe the partitioning of Al, Ca, K, Mg, O, S, Si, Th, and U (Equations 3 and 7). Unless otherwise noted, we treat all elements (except O) as exchange reactions. We considered a_i, b_i, and c_i terms for each element (Equation 3), the dependence for all elements on the O, Si, and S abundance in the metal (Equations S16–S19 in Supporting Information S1), self interaction in the metal for all elements, and all silicate Margules parameters (Equations S20 and S21 in Supporting Information S1) for interaction of each element with FeO, SiO_2 and CaO, a total of 78 potential terms. Note that, although fundamental properties of each reaction, the entropy, enthalpy, and volume of reaction (a_i, b_i, and c_i) are not known a priori and so must be found by fitting of the data. We did not weight samples according to experimental error so as not to bias the fit toward low pressure data. To enforce self-consistency, we fit the partitioning of every element in every sample at the same time. Given the complexity of the chemical system, there are likely degenerate combinations of parameters that would give similar fits to the data. Here we attempt to find a good fit to the data by sequentially excluding terms that are not statistically significant. Only terms that were statistical significant at the 95% level, as determined using an F-test (see Supplemental Information for details), were included in the final fit with the exception that the constant parameters a_i were included regardless to ensure stability of the parameterization. Of the possible 78 terms, only 48 were retained. The fitted parameters, covariance matrix, and correlation matrix are given in Tables S6–S8 of Supporting Information S2, respectively. The error on each fitted parameter can be extracted from the covariance matrix by taking the square-root of the corresponding diagonal term, but we suggest using the full covariance matrix as there are strong correlations between certain parameters.

The quality of our fit to the data compiled in Table S5 of Supporting Information S2 is demonstrated in Figure 2, where the calculated exchange coefficients are compared with the measured exchange coefficients for the elements examined in this study. The unweighted root-mean square (RMS) of the difference between the measured and calculated $\log_{10}K_D$ (i.e., residuals) for every element is 0.421 log units. Due to the larger number of experiments for which O, S and Si are reported, the cost function for the fit is more dominated by these elements; however, the quality of the fit for individual elements is good with RMS ranging from 0.325 to 0.593 log units (Table 3). Importantly, the quality of the fits for individual elements are comparable to fits that fit the data for each element separately including relevant silicate terms (RMS from 13% lower to 33% larger), and typically better than individual element fits that do not include a silicate activity model as typically used in many previous studies (RMS from 42% lower to 10% larger). It is worth noting that the global fit gives substantially better results for U compared to either of the individual element fits, suggesting the additional constraints on the silicate activity model and/or symmetric metal terms are import for correctly describing U partitioning.

To explore the suggestion by Badro et al. (2018) that Mg partitioning is better described by a dissociation reaction rather than an exchange reaction, we performed a separate fit in which Mg was described by a dissociation reaction (Equation 6) using the same approach. We find a similar, but slightly worse fit for all the data (RMS of 0.423 log units compared to 0.421 for exchange, Table 3) and for the partitioning of Mg specifically (RMS of 0.377 log units compared to 0.340). Several other elements are strongly affected by the treatment of Mg leading to a slightly different collection of statistically significant parameters and resulting in a slightly improved fit for O and Al but a worse fit for Ca, K and U. The influence of Mg is likely because the dissociation of MgO is closely

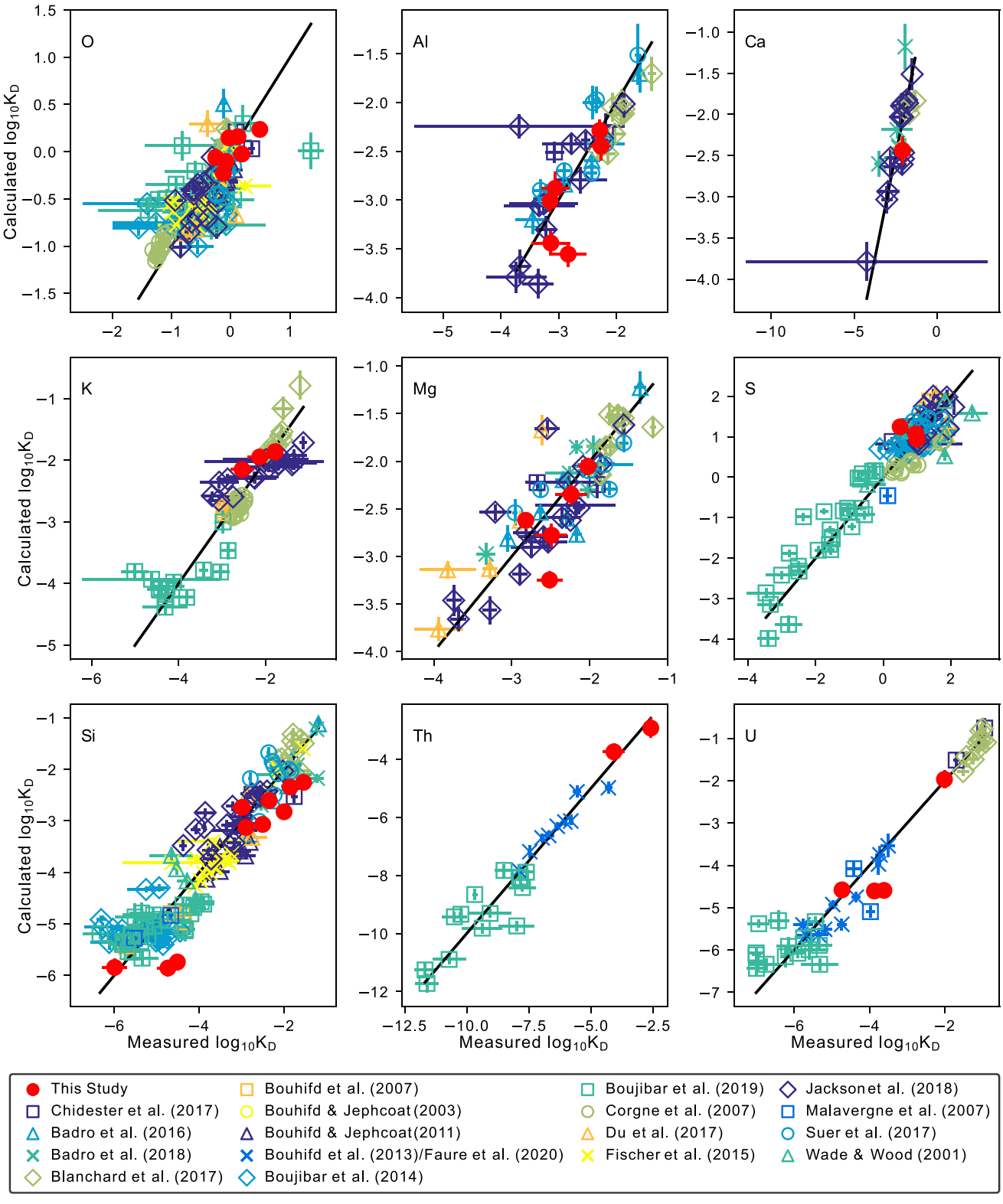

Figure 2. Calculated versus measured exchange coefficients for the elements fit in this study. Coefficients calculated from "Full fit with Mg as exchange", Table S6 in Supporting Information S2. Note that the data reported by Faure et al. (2020) was previously reported in Bouhifd et al. (2013) but without the Th measurements.

Table 3
Comparison of the Unweighted Root-Mean Square (RMS) Residual in Log Units for the Different Fits Discussed in Text: Complete Coupled Fits Including All Considered Terms for Mg as Exchange (Column 2) and Dissociation (Column 3) Reactions; a Similar Fit With Mg as Exchange but Not Considering Any Silicate Terms (Column 4); a Fit Considering No Metal or Silicate Compositional Terms (Column 5); and Fits Considering Just the Partitioning of Each Individual Element Including (Column 6) and Excluding (Column 7) Silicate Terms for That Element and FeO, CaO, and SiO_2

	N_{samp}	Mg as ex.	Mg as diss.	No sil.	No comp.	Ind. fit	Ind. fit, no sil.
Overall	196	0.421	0.423	0.513	0.742		
Al	146	0.348	0.329	0.352	0.472	0.235	0.325
Ca	42	0.359	0.376	0.398	0.575	0.257	0.398
K	25	0.353	0.349	0.456	0.593	0.294	0.456
Mg	64	0.340	0.377	0.328	0.543	0.235	0.306
O	57	0.325	0.320	0.359	0.383	0.332	0.332
S	115	0.467	0.466	0.655	1.120	0.437	0.612
Si	158	0.473	0.473	0.553	0.596	0.469	0.513
Th	25	0.593	0.604	0.765	1.655	0.470	0.842
U	42	0.527	0.539	0.647	0.760	0.598	0.647

Note. The number of samples for which there was partitioning data available for each element (N_{samp}) is also given in column 1.

tied to the partitioning of O, which is important for the partitioning of several other elements. Given that the choice of reaction with which to describe Mg partitioning only slightly alters the quality of our fits and that planetary growth calculations using the fits assuming exchange and dissociation for Mg give quite similar results (see below), it is not clear whether dissociation or exchange is governing the partitioning of Mg. Further data is likely required to resolve this debate.

To explore the influence of the compositionally dependent terms in our parameterization, in particular the silicate activity model, we also conducted two additional fits: one that did not consider any compositional terms for the silicate and another that did not include any compositionally dependent terms at all. As expected, these fits have higher residuals (RMS of 0.513 log units and 0.742 log units, respectively) with the large cations (Ca, K, Th, U), S, and Si most affected. In the end, our preferred parameterization is the full fit considering Mg partitioning as an exchange reaction (Table S6 in Supporting Information S2).

4. Implications for the Lithophile Element Budget of Earth's Core

To determine how lithophile elements may be affected by core segregation during Earth's accretion, we used our preferred metal-silicate partitioning parameterization within planetary growth models ("full fit with Mg as exchange", Table S6 of Supporting Information S2). We investigated two different scenarios: a single-stage core-mantle differentiation event, and a step-wise continuous growth model. The single-stage growth model assumes the whole core and mantle differentiated in one step at a single pressure, temperature, and fO_2 condition. Although not a physically realistic mode of core formation in planetary-sized bodies, it is often assumed that the composition of the mantle and core can be approximated by a single "average" equilibration using such a single-stage model. These models are a useful benchmark for comparison between studies and can provide insights into the systematics of metal-silicate equilibration in terrestrial planets. In the continuous growth model, the model planet grows by accretion of 100 equal-mass, differentiated bodies, and is intended to mimic oligarchic growth of planets. The mass fraction of the cores of the accreted bodies that equilibrate with the mantle of the growing planet (k) is uncertain and likely varies during accretion. We therefore consider two different scenarios where either the whole mass of the impactor core equilibrates with the planet's mantle ($k = 1$) or where $k = 0.3$ to account for a degree of inefficient equilibration as argued by several authors (e.g., Rudge et al., 2010).

We explore the effect of pressure and temperature on equilibration. In the single-stage models the total mass of the planet was equilibrated at between 20% and 60% of the final planets' CMB pressure (found iteratively). In continuous growth models, equilibration between the impactor's core and the entire (impactor plus target) silicate mantle occurred at between 20% and 60% of the CMB pressure of a non-rotating planet at each step (Note that a swiftly rotating planet, a condition expected after a giant impact, would have a much different pressure distribution than present-day Earth [Lock & Stewart, 2017, 2019]). In some cases, the highest P-T equilibration runs failed to converge due to strong feedbacks between the partitioning of different elements. For this reason, the lower temperature models tend to cover more P-T space in Figures 3–9. Maximal pressures of equilibration ranged from 55 to 83 GPa, consistent with previous studies (e.g., Fischer et al., 2015). In both linear and continuous planetary growth models, the temperatures of equilibration were set to either the temperature of the peridotite liquidus at the pressure of equilibration (Fiquet et al., 2010) or 1500 K above the liquidus temperature to simulate the effect of the very high temperatures expected after some impacts (e.g., Lock & Stewart, 2017; Stewart et al., 2020).

The composition of the accreting material in our models was derived from that of CI chondrites (Palme & O'Neill, 2013), but adjusted to be compatible with the bulk Earth as has been done previously (e.g., Fischer et al., 2015; Piet et al., 2017; Rubie et al., 2011). The refractory lithophile elements (Al, Ca, U, and Th) were

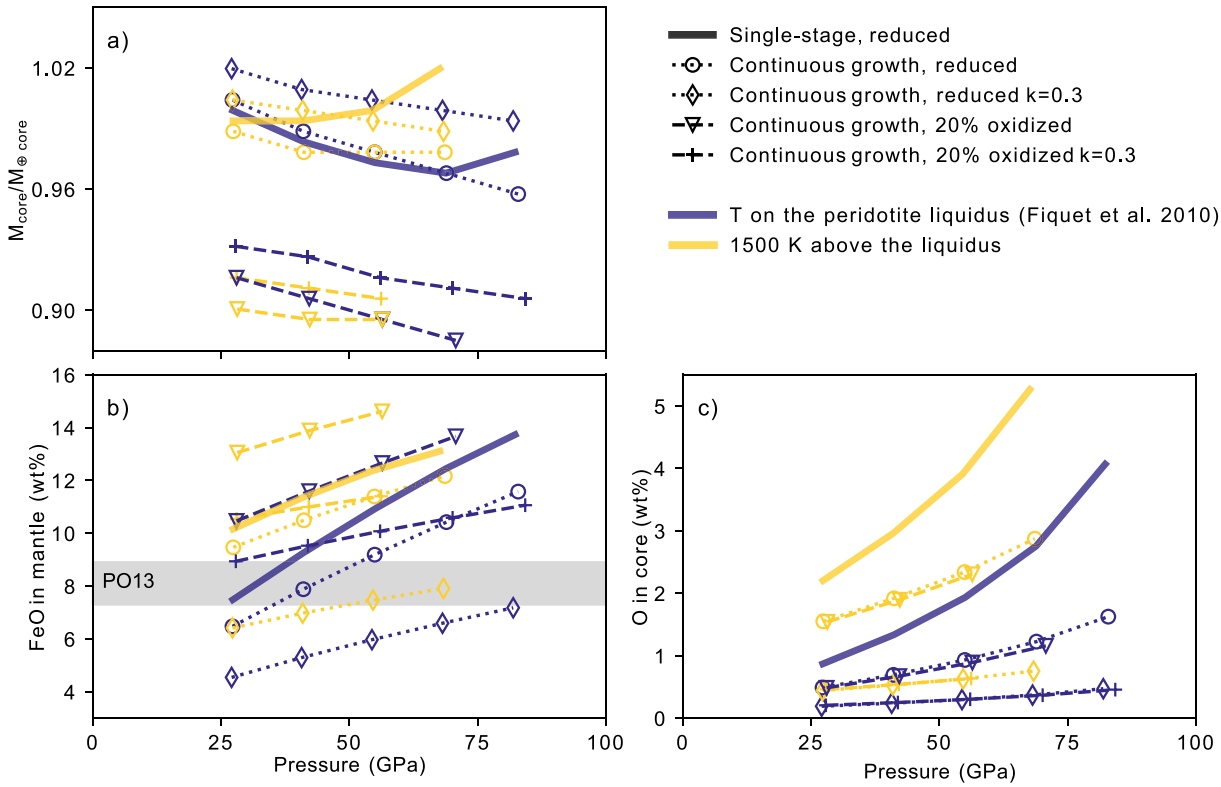

Figure 3. (a) Core mass, (b) FeO abundance in the mantle, and (c) O abundance in the core as a function of pressure found in our planetary growth models. Pressure is either the pressure of the single-stage equilibration or of the final equilibration step in a continuous growth model. *k* is the fraction of equilibrating metal (if different from 1). Equilibration occurred either on the liquidus (blue) (Fiquet et al., 2010) or 1500 K above the liquidus temperature (yellow). The Earth value (gray band) comes from Palme and O'Neill (2013).

enriched by 22% after Rubie et al. (2011) and K was depleted by 80% based on the volatile element depletion trend of Earth's mantle (Lodders, 2003). U and Th abundances were integrated back through time to 4.54 Gyr (25 and 450 ppb, respectively). Although it is well accepted that the composition of Earth is fractionated from that of CI chondrites in these elements, the exact degree of enrichment/depletion of Si, S and Fe were chosen as to give results from our planetary growth simulations that were roughly consistent with the core mass and mantle composition of Earth. Si was depleted by 8%, S depleted by 99.6%, and Fe enriched by 18%. We discuss the implications of these required depletions/enrichments below.

Emulating core formation in planetesimals, the adjusted-CI chondrite composition was then equilibrated at 0.1 GPa and 2000 K using partition coefficients calculated from our parameterization (Section 3.3). Oxygen was iteratively added to the system until the desired fO_2 was reached (IW-3.5 for reduced impactors and IW-1.5 for oxidized impactors). For the continuous growth models the composition of the metal was taken to be that of the cores of the accreting bodies and the composition of the silicate to be that of their bulk mantles. We do not consider silicate differentiation in our models and the silicate Earth is treated as a single, homogeneous reservoir. We ran one set of continuous growth models where all 100 impactors had the reduced composition, and one where the first 80 impactors were reduced and the last 20 impactors were oxidized. We will refer to models using these different histories of the composition of the accreted materials as reduced and oxidized models, respectively. A switch to a relatively oxidized population simulates mixing throughout the Solar System late in planet growth, as has been suggested by some authors (e.g., Rubie et al., 2011). While the composition of each type of impactor begins at a specific fO_2 (IW-3.5 for reduced compositions, IW-1.5 for oxidized), the fO_2 of the growing planet is allowed to vary self-consistently as metal-silicate partitioning of light elements occurs during growth (Fischer et al., 2015; Rubie, Jacobson, et al., 2015).

The pressure and temperature of equilibration, both within our experiments and within our models, are correlated because equilibration typically occurs at the liquidus temperature which is pressure dependent. Therefore, to help

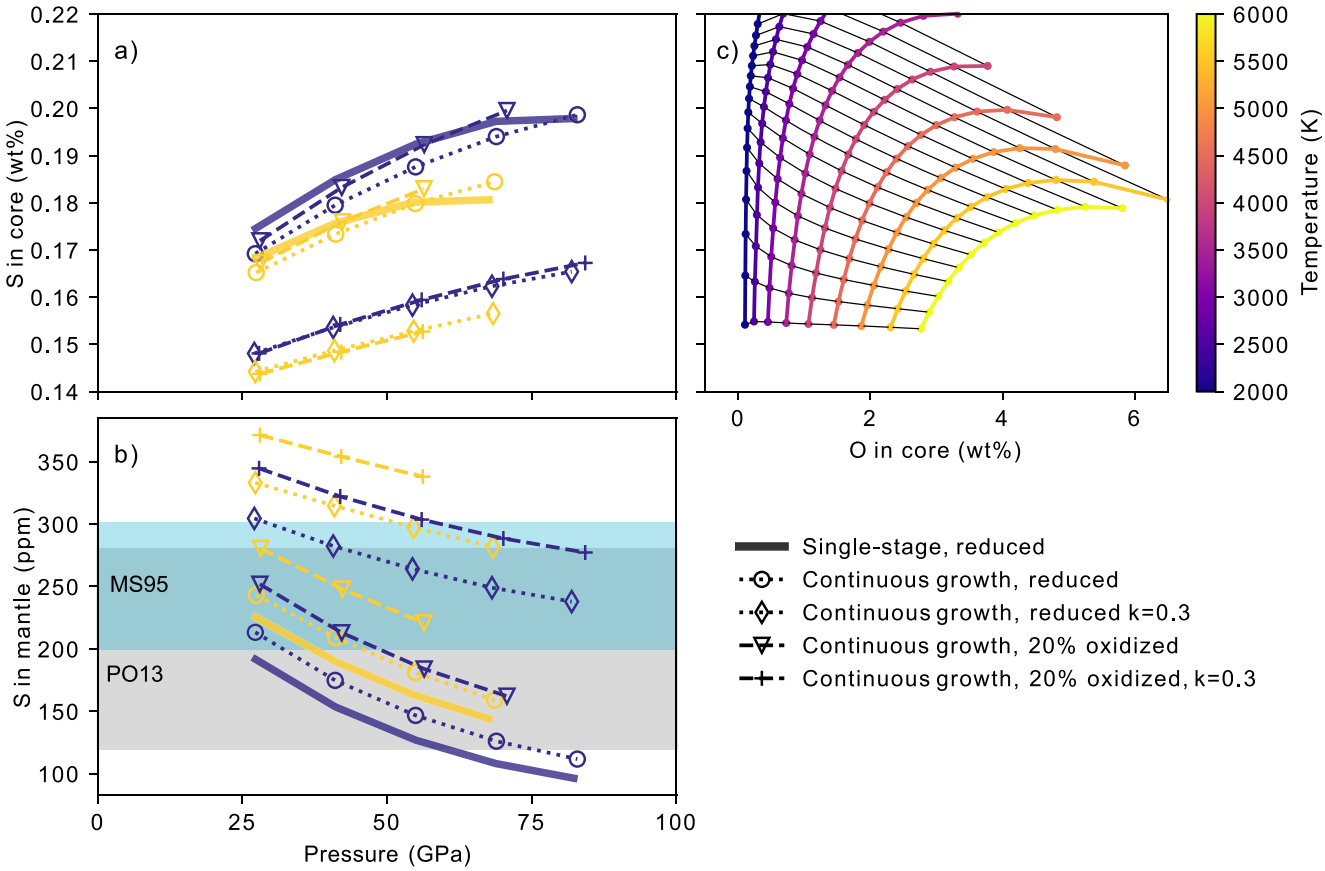

Figure 4. (a) S abundance of the core and (b) S abundance of the mantle as a function of pressure found in our planetary growth models. Symbols are as described in Figure 3. Temperature is either on the liquidus (Fiquet et al., 2010) (blue) or 1500 K above the liquidus (yellow) at each pressure. Mantle S values are from McDonough and Sun (1995) (teal) or Palme and O'Neill (2013) (gray). (c) Core S abundance as a function of O in single-PT models. Isobars (gray lines) start at 10 GPa and increase by 5 GPa with a max pressure of 130 GPa. The temperature in the single-PT models is indicated by the color bar.

separate the pressure and temperature dependence and to inform our discussion, we have conducted an additional series of calculations of metal-silicate partitioning using our parameterization (Section 3.3) at a range of fixed pressures (10–130 GPa) and temperatures (2000–6000 K). The bulk composition of the system was assumed to be that of the reduced impactors used in the planetary growth models. As with the planetary growth models, calculations did not converge in some regions of the parameter space. We will refer to these calculations as single-PT calculations. We now present the results of our planetary growth models, dividing our discussion into six sections addressing different elements or groups of related elements.

4.1. Metal-Silicate Partitioning of Iron and the Size of the Core

The mass of the core, and hence the corresponding abundance of FeO in the mantle, varies significantly between different planetary growth models (Figure 3a). The largest factor in determining the mass of the core is the oxygen fugacity of the starting material. The continuous growth models with late-accreted oxidized material have cores that are 88%–93% the mass of Earth's core, while the models with all reduced impactors have core masses between 96% and 102% Earth's core mass.

Within continuous growth models with a given impactor composition, the largest cores are the models with low equilibration constants ($k = 0.3$). This is because light elements are relatively incompatible in metal at the low pressures at which the accreting material was first equilibrated, and so the fraction of the cores of the accreting bodies that were added directly to the core of Earth brought comparatively little light element. In other words, if less metallic Fe equilibrates, less of that Fe will be replaced within the core by a lighter Si or O atom.

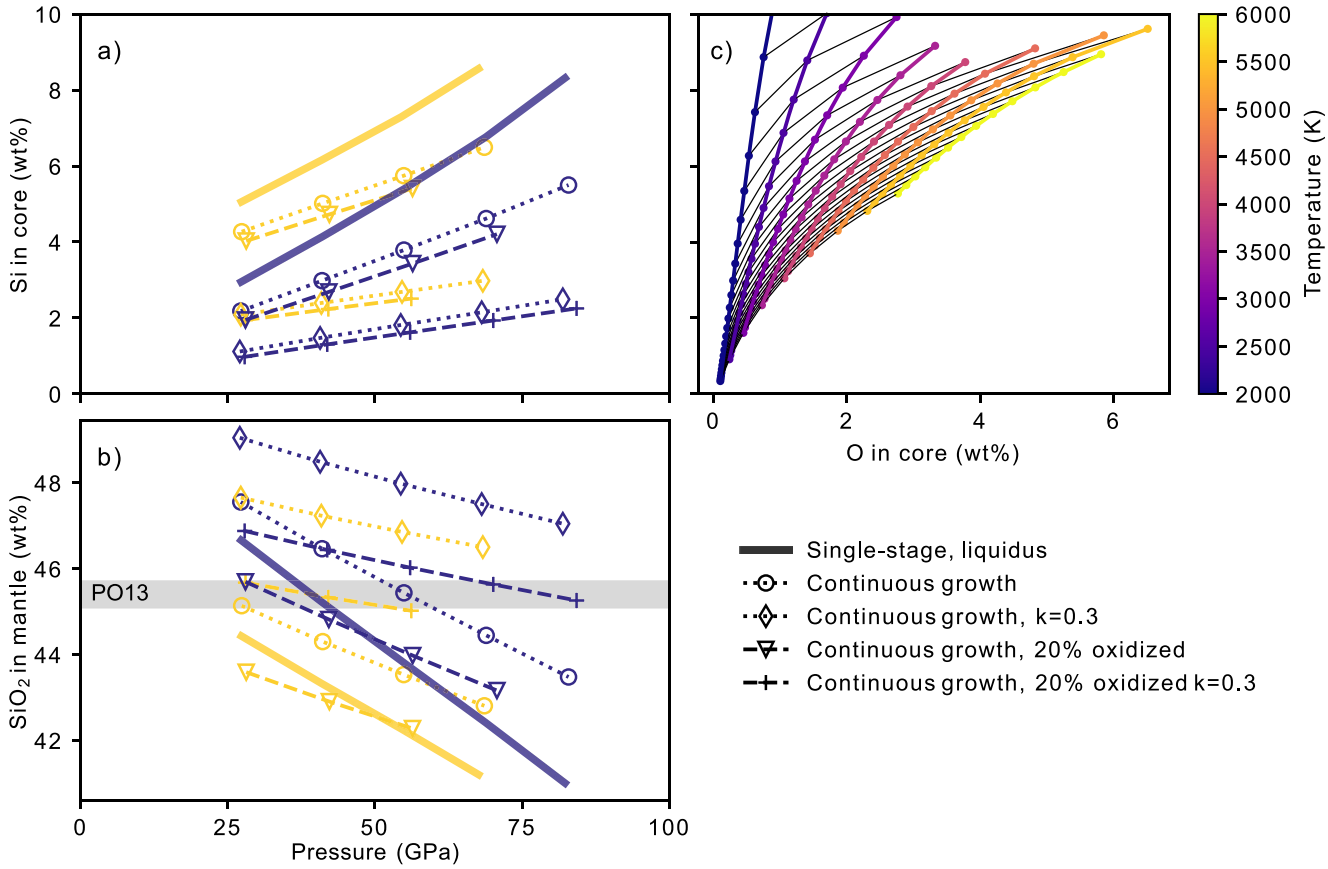

Figure 5. (a) Si abundance of the core, (b) SiO_2 abundance of the mantle as a function of pressure found in our planetary growth models. Symbols are as described in Figure 3. Temperature is either on the liquidus (Fiquet et al., 2010) (blue) or 1500 K above the liquidus (yellow) at each pressure. Earth values are from Palme and O'Neill (2013) (gray band). (c) Core Si abundance as a function of O in single-PT models. Isobars (gray lines) start at 10 GPa and increase by 5 GPa with a maximum pressure of 130 GPa. The temperature in the single-PT models is indicated by the color bar.

In continuous growth models, the core mass decreases as a function of equilibration pressure. For single-stage growth models the relationship with pressure is more complicated, initially decreasing the core mass and then increasing it, with the transition occurring earlier at higher temperatures. Temperature also has a complicated effect. Generally, increasing temperature decreases the mass of the core. However, in cases where material that has equilibrated at high *P-T* conditions makes a significant contribution to the composition of the core, such as in high pressure single-stage models or high-pressure continuous growth models where the entire impactor is equilibrated with the mantle, increasing temperature increases the mass of the core. This complicated *P-T* dependence is likely due to the competing effects of partitioning of different light elements into the core. For light elements which partition via the exchange reaction (Equation 2), adding light element to the core requires the extraction of heavy Fe and the core mass decreases. However, partitioning of oxygen is achieved by dissolution of FeO which carries both iron and oxygen out of the mantle and into the core, increasing the core mass. With increasing temperature and pressure, oxygen partitions more and more strongly into the core (Figure 3c, Section 4.2). At a certain point partitioning of oxygen begins to dominate and the mass of the core begins to increase with temperature. This transition is more pronounced, and happens at lower pressures (and therefore temperatures), in the single-stage models as the core's composition is set by a single, relatively high *P-T* equilibration rather than inheriting some of its mass from earlier, lower *P-T* stages of accretion.

Smaller cores are compensated by higher FeO abundances in the model mantles (Figure 3b). In general, we find that lowering the amount of Fe equilibration (i.e., $k = 0.3$) requires higher temperature equilibration to match both the core size and Earth's mantle FeO abundance. Similarly, all of our models with oxidized starting populations have an overabundance of mantle FeO, regardless of the equilibration temperature or k value. This highlights the convoluted effects of equilibration constant, temperature and bulk composition.

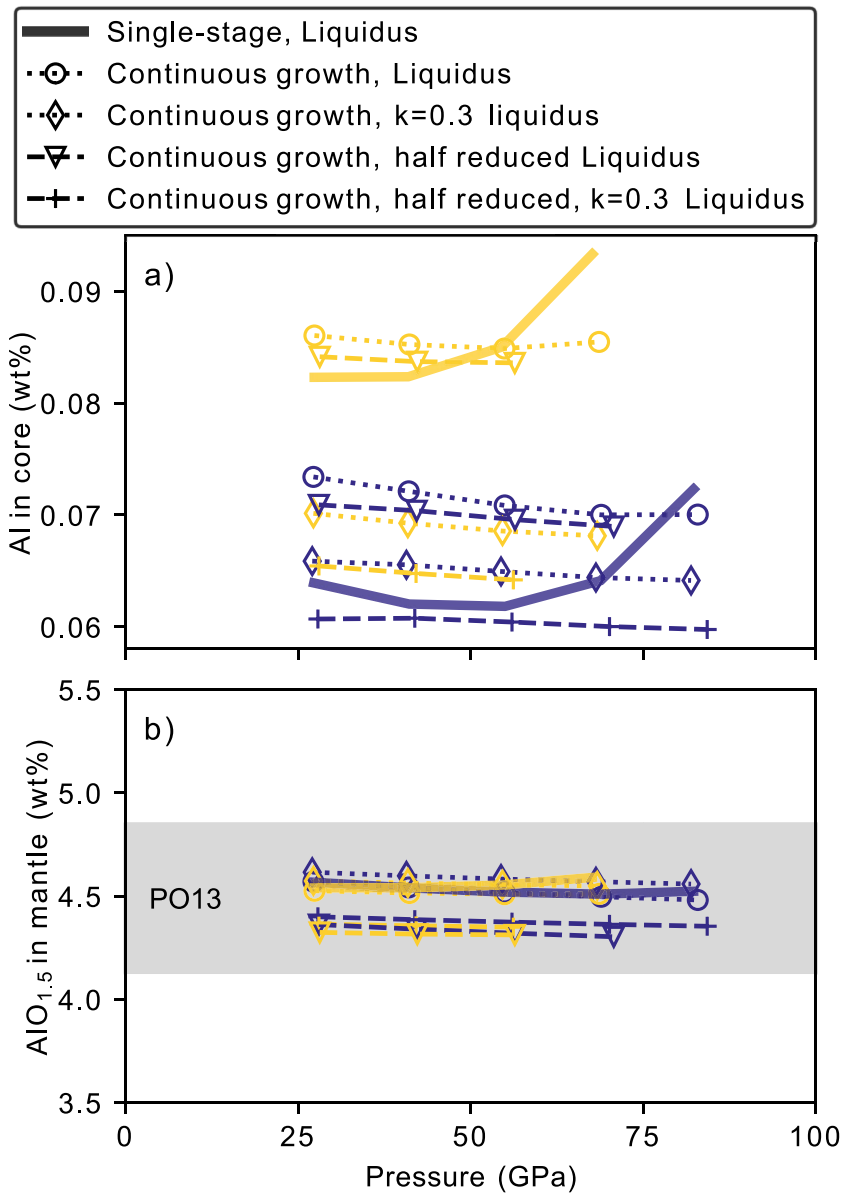

Figure 6. (a) Al abundance of the core, (b) $AlO_{1.5}$ abundance of the mantle as a function of pressure found in our planetary growth models. Symbols are as described in Figure 3. Temperature is either on the liquidus (Fiquet et al., 2010) (blue) or 1500 K above the liquidus (yellow) at each pressure. Earth values are from Palme and O'Neill (2013) (gray band).

4.2. Oxygen

The pressure and temperature dependence of O partitioning is enormously important for the partitioning of other elements, as we will discuss at length below. In our models, the partitioning of oxygen into the core increases significantly with increasing pressure and temperature (Figure 3c). Note, there is no direct pressure dependence resolved for O (i.e., $c = 0$). In this case, the observed pressure dependence in our models is likely due to a positive dependence on the Si content of the metal, which does have a resolvable c term (see Section 4.4). As a result, the single-stage equilibration models have a much higher range of possible core O abundances than the continuous growth models, and have generally much higher final core O abundances. While the continuous growth models reach a maximum O content in the core of ~2.5 wt%, the cores in the single-stage models are nearly double that amount. In a continuously growing planet, the core material equilibrates at a range of *P-T* conditions over the growth period, so the composition of the core will retain signatures from lower pressure

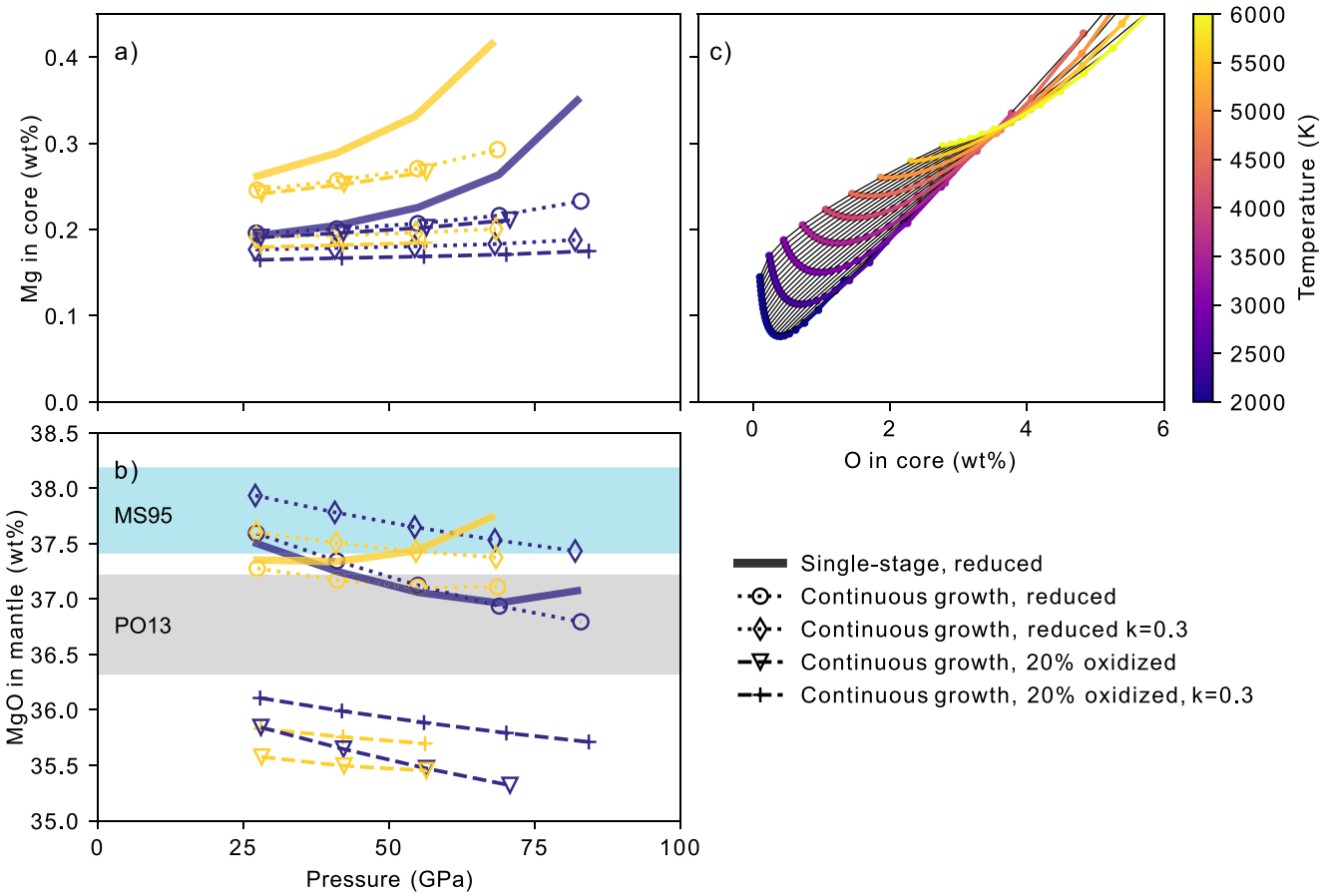

Figure 7. (a) Mg abundance of the core and (b) MgO abundance of the mantle as a function of pressure found in our planetary growth models. Symbols are as described in Figure 3. Temperature is either on the liquidus (Fiquet et al., 2010) (blue) or 1500 K above the liquidus (yellow) at each pressure. Mantle MgO values are from McDonough and Sun (1995) (teal) or Palme and O'Neill (2013) (gray). (c) Mg contents of the core as a function of O contents of the core in single-PT equilibration models performed at pressures between 10 and 130 GPa. The temperature in the single-PT models is indicated by the color bar.

(i.e., earlier) events. As expected, the O abundance in the core is lowest in disequilibrium accretion events (i.e., $k = 0.3$). Perhaps surprisingly, more oxygen in the system does not translate to more oxygen in the core. There is no substantial difference in O content of the metal between the oxidized and reduced continuous growth models when equilibration occurs at the same pressure and temperature conditions (Figure 3c).

The highest temperature and pressure conditions for core formation are expected to occur as a result of giant impacts near the end of Earth's accretion. In numerical simulations of giant impacts, much of the impactor's core typically merges with the target's core very quickly without extensive mixing with silicate material (Canup, 2012; Canup & Ashpaug, 2001; Cuk & Stewart, 2012; Lock & Stewart, 2017). However, the degree of equilibration between metal and silicate that could occur during merging of the cores is uncertain. Simulations of smaller impacts suggest that equilibration could be efficient due to stretching of the core and turbulent entrainment into the silicate (Kendall & Melosh, 2016; Lherm & Deguen, 2018), but the same processes are not as effective over the much larger scales of giant impacts (e.g., Landeau et al., 2016). If metal-silicate equilibration during giant impacts is indeed inefficient, k would, on average, be low during the late stages of planet formation and our models would suggest that the present-day core contains a relatively small amount of O (~0–2 wt%).

4.3. Sulfur

Sulfur is abundant in our Solar System, but because it is both volatile and moderately siderophile, its abundance within the bulk Earth is uncertain. S combines with Fe to form sulfides, which have been observed in relatively high abundances in some meteorites (Schrader et al., 2010). Since metallic meteorites are likely the remnants of

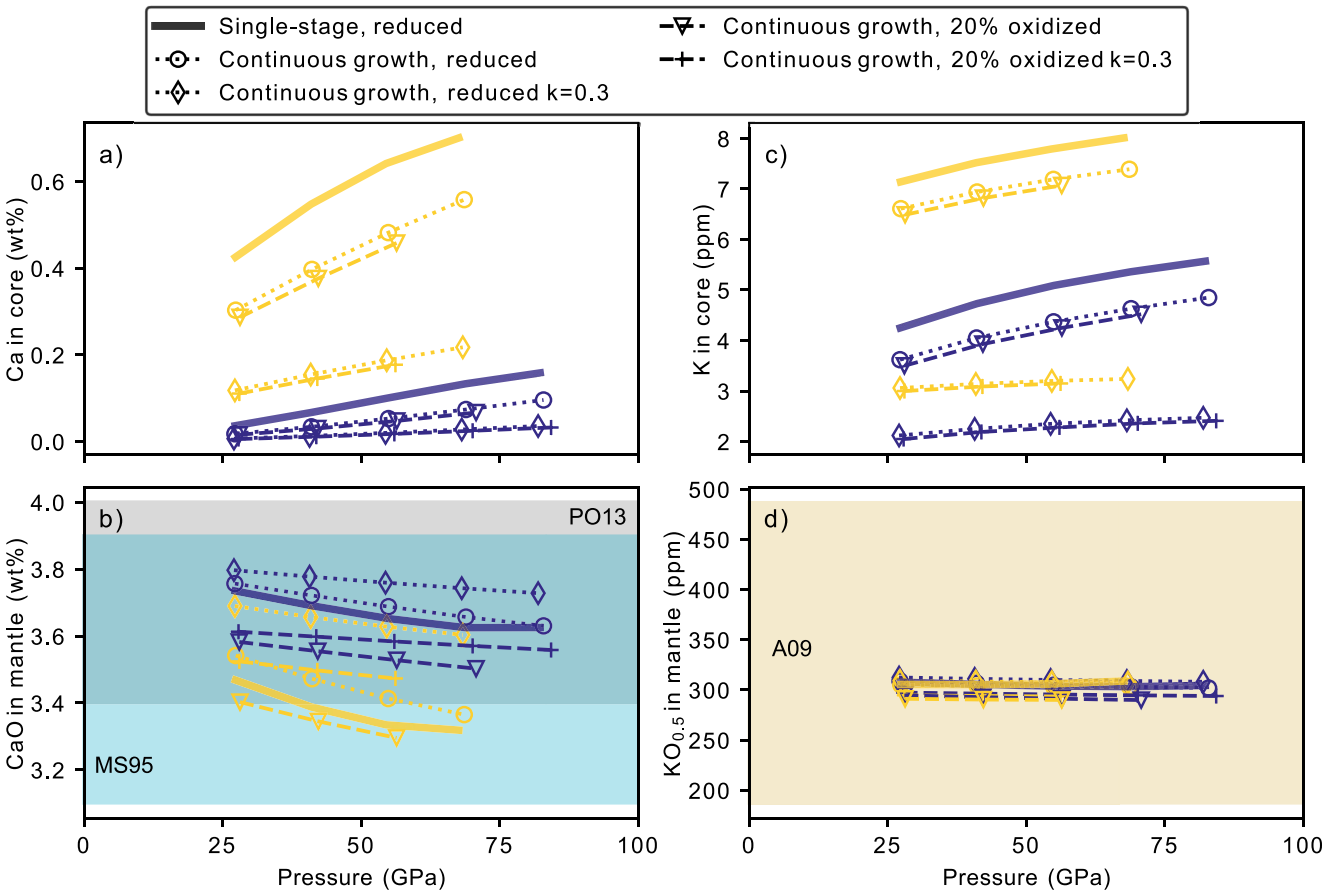

Figure 8. (a) Ca abundance in the core, (b) CaO abundance in the mantle, (c) K abundance in the core, and (d) $KO_{0.5}$ in the mantle as a function of pressure found in our planetary growth models. Symbols are as described in Figure 3. Temperature is either on the liquidus (Fiquet et al., 2010) (blue) or 1500 K above the liquidus (yellow) at each pressure. Mantle CaO values are from McDonough and Sun (1995) (teal) or Palme and O'Neill (2013) (gray). Mantle K value is from Arevalo et al. (2009).

the cores of ancient protoplanets (Goldstein et al., 2009), similar to those out of which Earth formed, it is possible that Earth could have accreted a large amount of S. S plays an important role in the cores of smaller Solar System bodies, and may also play a role in Earth's core. Additionally, the metal-silicate partitioning of chalcophile elements (e.g., copper, Mahan et al., 2018) may depend on the abundance of S in the metal phase during planetary differentiation (Bouhifd et al., 2013; Malavergne et al., 2007; Wohlers & Wood, 2015; Wood et al., 2014).

Our results for S partitioning are broadly similar to those reported by Boujibar et al. (2014) and Suer et al. (2017). The partitioning of S into the core is enhanced at high pressures, but inhibited at high temperatures (Figure 4). The pressure dependence is explicitly observed within our fit, as $c = 50 \pm 15$ K/GPa, but the temperature dependence is convoluted by chemical interactions. The explicit b parameter for S (Table S6 in Supporting Information S2) is negative, suggesting that increased temperature will be favorable for S partitioning into the core, but that is not what we observe (Figure 4). On the other hand, S partitioning is negatively dependent on the presence of both O and Si in the metallic liquid (i.e., ε_S^{Si} and ε_O^S are positive, Table S6 in Supporting Information S2), and both O and Si are strongly positively dependent on temperature. This is demonstrated in Figure 4c, where the core S abundance from single-PT calculations is plotted as a function of core O abundance. As temperature increases, the O abundance increases and S abundance mainly decreases. This is a clear demonstration of the need to consider the evolution of the whole chemical system when determining how the partitioning of a given element will change with pressure, temperature and composition.

To produce concentrations of S in the mantle that are consistent with the present-day estimates, it was necessary to use a starting composition that was significantly depleted in S relative to CI chondrites (Section 4). The low S

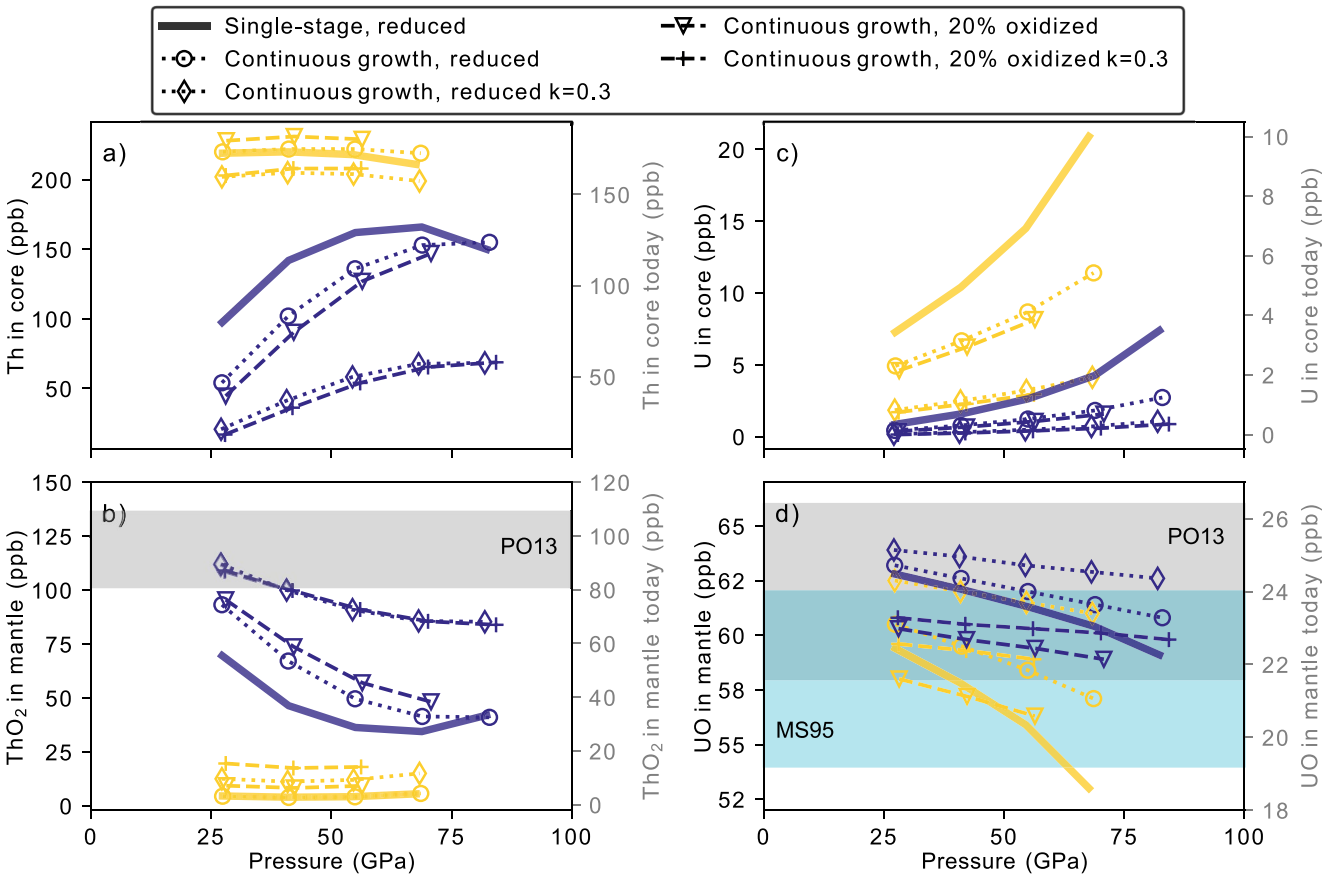

Figure 9. (a) Th abundance of the core, (b) ThO_2 abundance of the mantle, (c) U abundance of the core, and (d) UO abundance of the mantle as a function of pressure found in our planetary growth models. Left *y*-axes are the radioactive element contents at 4.56 Ga, right *y*-axes are the radioactive element content after radioactive decay to present day abundances. Symbols are as described in Figure 3. Temperature is either on the liquidus (Fiquet et al., 2010) (blue) or 1500 K above the liquidus (yellow) at each pressure. Mantle ThO_2 and UO values are from McDonough and Sun (1995) (teal) or Palme and O'Neill (2013) (gray).

contents in the metal we infer from our calculations suggests that the core is not a significant reservoir for S. The Earth must therefore have formed from material that was significantly depleted in S relative to CI chondrites and other meteorite groups or S must have been lost from the mantle by another mechanism other than core formation (e.g., O'Neill, 1991).

4.4. Silicon and Aluminum

Si^{4+} and Al^{3+} play a dominant role in the structure of the silicate melt. These cations coordinate with O anions to form tetrahedral units in the upper mantle and octahedral units in the lower mantle. The linking of these discrete polyhedral units determines the polymerization of the silicate melt. Because these elements inhabit the same crystallographic sites within the most abundant mantle silicates, it is logical that they should partition similarly into the metallic phase. However, they differ in terms of size and charge, which may also have an effect on their metal-silicate partitioning behavior.

The metal-silicate partitioning of Si into the core is strongly favored by increased pressure and temperature (Figures 5a and 5c). The Si abundance in our model cores ranges from 0.9 to 8 wt%. While the oxidation state of the starting material has very little effect on the Si abundance in the core, lowering the amount of equilibrating metal (as in the models with $k = 0.3$) decreases the core Si abundance significantly. As was observed with O partitioning, the continuous growth models result in cores with less Si than in single stage models due to the memory of lower *P-T* equilibration events. Increased partitioning of Si into the core is matched by a decrease of SiO_2 within the mantle (Figure 5b). The range of modeled SiO_2 contents is much larger than the range observed

in Earth's mantle, suggesting that, in conjunction with moderately siderophile elements, the abundance of Si in the mantle may be used as a constraint for the conditions of core formation.

The pressure dependence on the partitioning of Si has not been observed previously. However, we find a statistically significant pressure dependence on Si partitioning (i.e., $c \neq 0$, Table S6 in Supporting Information S2) even in parameterized fits where compositionally dependent terms were not included. Given that this data set is largely made up of past experiments, it is surprising that we resolve a pressure dependence when others have not. However, this may be the first time that all of these data sets have been used together, and given the number of samples, the large range in pressure, and the low root-mean-square for the fit, we believe the pressure dependence to be robust. Further, we find that Si partitioning is enhanced by the presence of O in the metal (Figure 5c). The interdependent partitioning of these two elements will serve to stabilize their presence within the metal phase. These results may have significant implications for the exsolution of SiO_2 from the core, as has been proposed by Hirose et al. (2017) and others as a means of driving a magnetic dynamo prior to inner core solidification.

On the other hand, the metal-silicate partitioning of Al is not dependent on pressure, but is highly dependent on temperature (Figure 6). Similar to Si, we observe very little dependence on the oxidation state of the starting material, but see a strong decrease in Al contents of the core when only 30% of the incoming metal is allowed to equilibrate. The total range of Al contents of the model cores is 0.06–0.09 wt% and, since so little Al is partitioned into the core, all of our models fall within the $AlO_{1.5}$ observed within the mantle. Therefore, we expect that core formation did not greatly affect the $AlO_{1.5}$ concentrations in Earth's mantle and the abundance of Al within Earth's core is low.

4.5. Magnesium

In contrast to the elements described previously, Mg is a major element that inhabits the A and B sites of silicate minerals, rather than the polyhedra defined by Si, Al, and O. Mg is often in solid solution with Fe and the Mg# (molar $Mg/(Mg + Fe^{total})$) is a key descriptor for minerals, rocks and terrestrial planets (e.g., Palme & O'Neill, 2013). Earth's primitive mantle has an inferred Mg# of 0.890 and an Mg/Si ratio of 1.04. Mg could also play a significant role in the dynamics of Earth's core as exsolution of MgO from the core over time may help drive the magnetic dynamo (Badro et al., 2016; O'Rourke & Stevenson, 2016).

In our core formation models, the Mg contents of the metal increases as equilibration pressure and temperature is increased (Figure 7a). The Mg fit does not have an explicit pressure dependence ($c = 0$) and the temperature dependence represented by the b term in Equation 3 is unfavorable for Mg partitioning into the metal (i.e., $b = 4000 \pm 2000$ K). Thus, the pressure and temperature dependences observed for Mg are entirely due to its interaction with O in the metal phase and the activity of the silicate melt. Figure 7c shows the Mg abundance in the core as a function of O abundance in the metal from our single-PT calculations. At low temperatures, the Mg contents within the metal decreases as a function of pressure and increasing O due to changes in the silicate melt structure. However, the increasing O content of the metal as a function of temperature drives a large increase in the Mg content of the metal. While the independence of Mg partitioning from temperature is in direction contrast to some previous studies (e.g., Badro et al., 2016, 2018), it is similar to the findings of Du et al. (2017), who also found a strong dependence on the O content of the metal for the metal-silicate partitioning of Mg.

On the other hand, the MgO concentration in the mantle show a much stronger dependence on the starting material and on pressure, both of which are likely due to the change in the total mass of the mantle, given the relatively small amount of Mg partitioned into the core (Figure 7b). Indeed, to avoid underestimating the MgO concentrations in the mantle we found that the Si content of the starting material must be depleted by at least 8% relative to CI chondrites (therefore increasing the starting Mg/Si ratio, see above and Section 5.2). Additionally, the models that have 20% oxidized bodies in the starting population have an overabundance of FeO and an underabundance of MgO in their mantles. These results are robust regardless of whether Mg partitioning is treated as a dissociation reaction or as an exchange reaction.

4.6. Calcium, Potassium, Thorium, and Uranium

At high pressures in Earth's lower mantle, the cations Ca^{2+}, K^{1+}, U^{2+} (Blanchard et al., 2017; Chidester et al., 2017), and Th^{4+}, are expected to be enriched in Ca-silicate perovskite or similar accessory phases (e.g., Corgne, 2002;

Corgne et al., 2003, 2005). This is due to their large size and despite the considerable charge balancing required for 4+ cations (e.g., Th). Thus, we would expect these elements to behave similarly in metal-silicate partitioning situations.

All four of these cations have strong positive dependencies on the temperature of equilibration (i.e., b is large and negative, Table S6 in Supporting Information S2). This temperature dependence is exhibited in the planetary growth models (Figure 8). When equilibration occurs on the liquidus at each step, the maximum Ca abundance in the model core is 0.16 wt%. On the other hand, when equilibration occurs at 1500 K above the liquidus temperature, the maximum Ca abundance is more than four times higher (0.71 wt%), although these results are extrapolated somewhat beyond the range over which the partitioning of Ca is experimentally constrained (Section 5.1). Consequently, the CaO abundance in the mantle decreases when metal-silicate partitioning occurs at higher temperature, an effect that is compounded by the changing mass of the mantle. Overall, the modeled abundances of Ca in the core are quite low (<1 wt% for all cases, Figure 8a) and we are able to match Earth's observed mantle abundance of CaO regardless of equilibration conditions (Figure 8b).

Similarly, the K abundances in the model cores are higher when equilibration occurs at high temperature (Figure 8c), but are quite low overall (maximum of ∼8 ppm). Although the K abundance within the model core varies by a factor of ∼4 dependent on the metal-silicate equilibration conditions, only a small change in the K abundance is registered within the mantle (Figure 8d). In terms of the absolute abundance of K in the mantle, a depletion of K in the starting material of 80 wt. % relative to CI, as used here, is easily accommodated given the large uncertainty in the mantle's K abundance.

Thorium partitioning is also strongly and favorably dependent on temperature (Figure 9). The cores of our model planets contain between 20 and 250 ppb Th, with the lowest abundances observed in the low-temperature, incomplete equilibration examples. When equilibration occurs at 1500 K above the liquidus, all model cores contain ∼200 ppb Th. These model abundances are likely unreasonably high (Figure 9a). Indeed, we are unable to match the mantle abundance of ThO_2 in almost all cases because so much Th is sequestered into the model core.

Qualitatively, we find Th to be one of the most strongly "lithophile" elements in our experiments. For example, of the seven Th-bearing samples in our study only two had measurable Th contents within the metal phase. Additionally, all Th-bearing samples in this study exhibited a Th- and Ca-rich mineral outside of the silicate melt region (Figure 1), suggesting Th is more compatible in the solid silicate phase than in the liquid at these high P-T conditions. While this behavior is somewhat puzzling, as Th is considered an incompatible element at surface conditions (i.e., partitions into the silicate melt phase), the result is that there is much less metal-silicate partitioning data available for Th than for any other element except for Ca. Importantly, although our parameterization gives a good fit to our experimental data (Figure 2), the only high-temperature (>∼2400 K), high-pressure (>8 GPa) data for Th are the two samples reported in this study, so there are very little data to constrain partitioning at the conditions of the planetary growth models. Therefore, the Th partitioning in the planetary growth models is a significant extrapolation from experimentally well-constrained compositions and thermodynamic states leading to an over-dependence on the equilibration temperature. Thus, we will not draw conclusions as to the Th content of Earth's core from our models, other than it is likely much lower than our models suggest. Given the very low abundance of Th in natural systems, the elevated partitioning within our models should not greatly affect the partitioning of any other elements. In the future, a more complete thermodynamic description of the metal-silicate partitioning of Th will benefit from chemical analyses with very low detection limits and high spatial resolution and better characterization of how the high-Th Ca-mineral seen in Th-rich experimental products affects partitioning.

There is much more experimental data on the metal-silicate partitioning of U, particularly over the range of pressures and temperatures found in the planetary growth models, making the parameterization of its partitioning more robust. There is a slight increase in the core abundance of U as the pressure of equilibration is increased, but this likely mostly due to the increased temperature of equilibration as pressure is increased. Recall that pressure and temperature are correlated in both the experiments and in the models because the liquidus temperature is pressure dependent. U partitioning depends very strongly on temperature, with a 5- to 10-fold increase in the U core abundance with a 1500 K increase in equilibration temperature for the continuous growth models. We are able to match the Earth's mantle abundance of UO for even the very high temperature models, suggesting that the core could host a significant amount of U without leaving a detectable mantle signal.

It is important to note that wile the UO_2 abundances in our starting materials are much higher than natural abundances, we find that Henry's law is satisfied even in the most extreme case. We conducted four metal-silicate partitioning experiments on U to explicitly address the overabundance of this element in our samples (PC samples in Table 1). In these samples, the UO_2 in the starting material was varied by two orders of magnitude (0.1–12 wt. %), yet the partition coefficients ($D^U = x_U/x_{UO}$) for these samples varies only by 0.4 log units (see Tables S3 and S4 in Supporting Information S2 for molar concentrations in these samples). This suggests that the partitioning of U is insensitive to the abundance of U in the sample and that experiments with a wide range of UO_2 abundances are valid.

5. Discussion

5.1. A New Parameterization for Metal-Silicate Partitioning

This is the first study to fit a parameterization for the metal-silicate partitioning data of nine elements simultaneously, an approach that was made possible by collating a large number of experimental studies. The results of our parameterization and planetary growth models highlight the importance of considering the behavior of the whole chemical system simultaneously. Elements that have explicit dependencies in, say, temperature (i.e., a non-zero *b* parameter) may have much more modest, or even the reverse dependence on the same parameter when the whole chemical system is considered. The best example of this is Mg where an explicit temperature dependence that would not favor partitioning is entirely overwhelmed by the fact that Mg partitioning is dependent on O concentration in the core and that O concentration increases strongly with temperature (Section 4.5). To accurately describe the behavior of different elements during core formation, it is necessary to fit multiple elements simultaneously and to include these complicated interdependences between those elements.

Fitting a large number of elements, including the major elements, simultaneously and using a large collection of experimental data has also allowed us to include, and constrain, a simple silicate activity model in our parameterization. We can therefore explore which elements are most sensitive to the silicate melt structure. Unsurprisingly, the inclusion of additional fitting parameters through the silicate activity model (48 statistically significant parameters for the full model vs. 33 for the model that did not include the silicate activity model) improves the quality of the fit for almost all elements (with the exception of a slight decrease in the fit quality for Mg, Table 3). However, the improvement is particularly great for the large cations K (22%), Th (22%), and U (19%), and S (29%). In fact, the fit for U in our combined model is better than when fitting U partitioning in isolation, suggesting that the additional constraints on the silicate activity model provided by the partitioning of other elements are important for correctly describing U partitioning.

While larger and higher valence cations (K, Th, and U) are expected to be responsive to the silicate melt structure (O'Neill & Eggins, 2002; Stebbins et al., 1984), the sensitivity of S to the inclusion of the silicate melt model is more surprising. In our model, we have assumed that S is a lone element with valence 0 and is partitioned through a dissolution reaction. However, S is an incredibly redox sensitive element and can have many different valence states between −2 and +6. A change in the valence state of S would fundamentally change the mechanism by which it partitions. We hypothesize that the statistically significant dependence of S partitioning on FeO, SiO_2 and CaO in our silicate activity models is an indication that the partitioning of S is dependent on the oxygen fugacity of the system. More work is needed to understand the valence state (i.e., speciation) of S, and therefore the mechanism by which S partitions between metal and silicate, in experiments at the conditions of core formation.

It is important to reiterate that the silicate activity model used in our parameterization is not an accurate description of the absolute activity of the melt. This is evidenced, for example, by the consistently large activity coefficients for FeO that lead our model to predict likely unrealistically high $f\,O_2$. While our γ_{FeO} at the conditions relevant for Earth formation are typically 3–5, previous studies have consistently found $\gamma_{FeO} \sim 1.5$ (Holzheid et al., 1997; O'Neill & Eggins, 2002). Our silicate activity model is missing several key components, including pressure and temperature dependencies on the Margueles parameters and non-symmetric interaction terms between the oxides. Much more experimental data, particularly at high pressures and temperatures, is required to constrain a more complete model and so this is left to future work.

Any parameterization is only as good as the data that is used to constrain it. In Section 4.6 we discussed the scarcity of data for Th at the high pressures and temperatures expected during much of planet formation, but there

are also other elements for which parts of the pressure, temperature and composition space that are relevant for core formation that are not well constrained by experiments. For example, it is notoriously difficult to control the oxygen fugacity in DAC experiments and most of the experimental data at high temperatures and pressures have high O concentrations in the metal. The results of our super-liquidus single-stage planetary growth models (which have equilibration temperatures >~5000 K) produce cores with O concentrations of <~5%, below most of the high temperature experiments at the same temperature. Similarly, the highest temperature experiments that measured Ca partitioning (~5000 K) are below the temperatures reached in super-liquidus planetary growth models. Therefore, further experimental studies of the metal-silicate partitioning at high temperatures, particularly of samples containing Ca, Th, and U, are required to better constrain metal-silicate partitioning over the range of conditions relevant for core formation. Additional data could also be provided by reanalysis of experimental samples to determine the partitioning of nominally lithophile elements such as Ca and Al. It must be stressed that use of any parameterization much beyond the region in which it is experimentally determined is inadvisable.

5.2. The Effect of Core Formation on the Composition of the Mantle and Core

How elements partition between the mantle and core during core formation plays a significant role in determining Earth's subsequent evolution. Furthermore, the abundances of different elements in the mantle today is often used to infer the composition of the material from which Earth accreted and, combined with models of core formation, the composition of the core. Here we will use the results of our planetary growth models to discuss the effect of core formation on the chemical structure of Earth and the implications for interpreting observations of the terrestrial mantle. It is important to note that none of our models produced a planet that was an exact match for Earth, which is not surprising given the simplified growth histories we have considered. Our approach therefore is to discuss the magnitudes of the mantle and core concentrations we find in our models, their trends with pressure and temperature of equilibration, and the effect of the bulk composition of accreting material.

To first order, the size of the core and the oxidation state of the mantle are set by the bulk composition of the accreted material and the partitioning of Fe. To produce a sufficiently large core and the terrestrial mantle FeO content in our planetary growth models that assumed a reduced starting condition (IW-3.5), it was necessary to have a starting material that was enriched by 18% in Fe relative to CI chondrites. Any addition of oxidized material would require a larger Fe enrichment to produce a sufficiently large core which would exacerbate the fact that the addition of too much oxidized material leads to a mantle that is enriched in FeO (as in our 20% oxidized continuous growth models). Our results therefore support the conclusion which has been made based on several isotopic systems (Dauphas et al., 2014) that carbonaceous chondrites are not the building blocks of Earth and that a significant portion of Earth's mass came from more reduced populations, such as enstatite chondrites.

Metal-silicate partitioning of light elements into the core has a second-order effect on the mass of the core. We observe higher abundances of lithophile elements in the core when equilibration occurs at high pressures and high temperatures. When lithophile elements are partitioned as an exchange with Fe, as in the case of Si, then increased pressures and temperatures result in a decrease in the density and the related mass of the core. On the other hand, when partitioning occurs as a dissolution, as in the case of O, then Fe is added back to the core along with the light element, and increasing the pressure and temperature of partitioning has a much smaller effect on the density of the core. Our models predict O and Si abundances within the core of up to ~5 wt% and 8 wt%, respectively, within the range of values predicted by previous studies (Fischer et al., 2015, 2017; Hirose et al., 2017; Rubie, Nimmo, & Melosh, 2015). Similar to previous studies, we find that Si and O are mutually beneficial for partitioning, such that increasing the abundance of one of the elements in the core increases the abundances of the other. In the past, this interaction has proven a challenge in continuous planetary growth models, because the ε-formalism used in the parameterization is relatively unstable under extrapolation to high pressure and temperature, and the mutual interactions of Si and O can cause the models to run away (e.g., Fischer et al., 2015). To mitigate this issue, we used strongly buffered stepping in the equilibration calculation in our planetary growth models and demanded that each of the partitioning equations (Equations 3, 5, and 7) be satisfied at each step. However, even with these precautions, growth models still fail when the solutions are far beyond the conditions well constrained by experiments (such as high pressure and temperature), which we think is again due to strong interactions between different elements. Simpler functional forms, that are more stable under extrapolation, must be used to explore core formation under more extreme *P-T* conditions (e.g., in a giant impact).

On the other hand, although S partitioning into the core is enhanced at high pressure, it is inhibited at high temperatures. As discussed in Section 4.3, this effect is likely due to strong and negative correlations with the Si and O content of the metal phase. In the past, the very low abundance of S in Earth's mantle has been attributed to the combined effects of its highly volatile nature and its siderophilic behavior in lower pressure systems. Thus, whatever S exists in the mantle is what is left over after incomplete accretion of volatile elements and core segregation. We find that to match the Earth's mantle abundance of S (Figure 4c), the bulk S of the chondritic starting material must be depleted by 99.6% (resulting in a total abundance of 216 ppm in the starting material) and very little S is partitioned into the core (~0.2 wt%). This result suggests that core formation plays a very minor role in the S depletion in Earth's mantle and rather the lack of S within Earth's mantle is due to volatilization during accretion of the planet or a S-poor source material. An important caveat, however, is that our parameterization does not account for silicate–sulfide or metal-sulfide partitioning of S. It is possible that sulfur was segregated out of the mantle as a sulfide, rather than a metal (e.g., the "Hadean matte" [Ballhaus et al., 2017; Laurenz et al., 2016; O'Neill, 1991; Righter et al., 2018, 2020; Rubie et al., 2016]).

Adding up the core abundance of all elements lighter than Fe (Al, Ca, K, Mg, O, and Si), we find that the total abundance of light elements in our model cores ranges from 1.5 to 10.5 wt% in continuous growth scenarios and up to 14 wt% in single-stage models, the vast majority being O or Si. The unique combination of light elements in Earth's core must match the seismically observed density (5%–10% less than pure Fe in the outer core with a 4.5% increase at the inner core boundary [Anderson & Isaak, 2002; Birch, 1952; Shearer & Masters, 1990]) and bulk sound speed (Dziewonski & Anderson, 1981). Recent ab initio calculations suggest that an O abundance of 5.4 wt% alone can fulfill both the density requirements and the bulk sound velocity, but the best numerical solution contains 3–4 wt% O, a small amount (~1–2 wt%) of Si and very little S or C (Badro et al., 2014). On the other hand, our models suggest that more Si can be partitioned into Earth's core than O, but are otherwise not inconsistent with these previous findings. Undoubtedly, these estimates will be updated as more experimental data on materials properties at core conditions becomes available.

The composition of the mantle is also affected by core formation. In particular, our planetary growth models produce planets with mantle SiO_2 and FeO abundances that cover a wide range relative to the range of estimates for the terrestrial mantle, depending on the mode of planetary growth and the pressure and temperature of equilibration. Significantly, the concentrations of SiO_2 and FeO have opposite dependencies on the pressure and temperature of metal-silicate equilibration (Figures 3 and 5). This suggests that, in addition to the commonly used moderately siderophile elements (e.g., Fischer et al., 2015; Siebert et al., 2012), measurements of mantle SiO_2 and FeO contents could be a powerful constraint on the core formation history of Earth.

Metal-silicate partitioning of Si has been invoked to explain the high Mg/Si ratio in Earth's mantle when compared to CI chondrites (e.g., McDonough & Sun, 1995). In our core formation models we see a significant amount of Si partition into the core, but only modest amounts of MgO, significantly changing the Mg/Si ratio of the mantle. However, the differential partitioning between these two elements is unable to account for the Earth's mantle Mg/Si ratio using core formation alone. Indeed, matching Earth's mantle abundances of MgO and SiO_2 required our model bulk composition to be depleted in Si by 8%–10% (see Section 4 for a discussion on the model starting composition). These results are in line with the findings of Dauphas et al. (2015), who used Si isotope systematics to infer that, in addition to the core formation process, Earth's mantle Mg/Si ratio is a result of nebular fractionation of forsterite. Their results suggest that Earth's core holds a modest ~3.6 wt% Si, very similar to our model results.

The mantle abundances of other lithophile elements (such as Mg, Al, Ca, K) are in general less affected by the pressure or temperature of equilibration, because they partition only weakly into the core. Instead, the dominant effect that leads to changes in the mantle concentrations of these elements is the variation in the mass of the core due to Fe, O and Si partitioning. This type of variation on mantle composition due to variable core size has also been noted previously for moderately siderophile elements (Righter, 2002).

A key feature of more realistic planetary growth models is that the core and mantle inherit much of the composition from the earlier stages of growth, when the pressure and temperature of equilibration were lower. In single-stage core formation models, the partitioning of elements is dictated by a single peak pressure and temperature event. In continuous evolution models, however, only a fraction of the material in the core experienced the same high pressure and temperature conditions. As a result, the mantle and core compositions of single-stage growth

models span a potentially much wider, and sometimes different, range than in the more realistic core formation models. This effect is particularly noticeable in cases where metal equilibration is incomplete (i.e., $k \neq 1$) and a large fraction of the final core's mass is inherited directly from the core of the (often much smaller) impacting body. The highest pressure and temperature conditions for core formation likely occur during and in the aftermath of giant impacts. As discussed above, in such events much of the core of the impacting body may not equilibrate efficiently with the proto-Earth's mantle (i.e., $k \ll 1$, e.g., Carter et al., 2020; Landeau et al., 2016) and Earth's core likely inherited a strong memory of its earlier accretion. Therefore, the effect of core formation on the composition of Earth's mantle and core cannot be accurately determined using an "average" pressure and temperature of equilibration, as has often been done (e.g., Chidester et al., 2017), and the complicated dynamics of metal-silicate partitioning in accretionary processes must be considered.

5.3. Implications for the Energy Budget of the Core and Powering the Magnetic Dynamo

The composition of Earth's core controls its ability to produce a magnetic field. At present, the magnetic dynamo is driven by chemical convection as light elements are excluded from the crystallizing inner core (e.g., Nimmo, 2015b). Prior to inner core nucleation, the energy structure of the core is less well constrained. Assuming no other chemically derived energy sources, thermal convection must have been driven by conductive heat flow out of the core (i.e., secular cooling). If the conductivity of the core alloy is very high (e.g., de Koker et al., 2012; Pozzo et al., 2012), that would suggest that the core has been cooling very rapidly, and the inferred initial temperature of the CMB is well above the liquidus temperature of the mantle. Instead, it has been proposed that precipitation of low-density oxide material (MgO, SiO_2) at the CMB as Earth cooled could have helped power a dynamo for much of Earth's history without the need to rely on conductive cooling (e.g., Hirose et al., 2017; Nimmo, 2015b; O'Rourke & Stevenson, 2016; O'Rourke et al., 2017). Additionally, heat produced by the decay of radioactive elements (such as U, Th, and K) in the core would slow the cooling of the planet, meaning that modeled CMB temperatures early in Earth's history would be much lower than those required to drive a geodynamo through conductive heat loss without this additional heat source. We can use our metal-silicate partitioning parameterization and planetary growth models to constrain the realistic range of compositions for Earth's core and hence the role different chemical processes can play in the dynamics of the core.

Some recent studies have suggested that SiO_2 would have precipitated out of the core early in Earth's history as the planet cooled and provided energy to power Earth's magnetic field (e.g., Hirose et al., 2017). For such a process to work, sufficient Si and O must be incorporated into the core during accretion so that the core reaches saturation, and SiO_2 must become more insoluble in the core as its temperature decreases. In support of this potential mechanism we find that the partitioning of both O and Si are both positively dependent on temperature. Additionally, several wt% Si and O can be partitioned into the core during accretion and both Si and O can be incorporated in significant amounts simultaneously (Figure 5c), similar to the conclusions of some other studies (Fischer et al., 2015). However, we find that Si partitioning into the metal is favored at high pressures (Figure 5), so the concentrations of Si and O partitioned into the core by equilibration at mid-mantle pressures (as suggested by moderately siderophile element partitioning, Fischer et al., 2015; Siebert et al., 2012) may be insufficient to cause SiO_2 saturation in the core at the high pressures of the CMB. Given the strong temperature dependence of Si and O partitioning, if a large fraction of the core equilibrated with mantle material at very high temperatures and/or pressures it may still be possible to oversaturate the core in SiO_2. Thus, for SiO_2 precipitation to be a significant energy source for the terrestrial dynamo, a planetary growth pathway where a large fraction of core formation occurred at high temperatures and/or high pressures is required. Given that such equilibration conditions are only expected toward the end of planetary growth in giant impacts when the equilibration constant of the metal, k, is expected to be lowest, we do not expect precipitation of SiO_2 in the core.

Similarly, elevated Mg partitioning at increased temperatures and subsequent MgO precipitation during core cooling has been proposed as a way to drive Earth's magnetic field (Badro et al., 2016; Mittal et al., 2020; O'Rourke & Stevenson, 2016). Models suggest that several weight % Mg are required in the core after accretion to saturate core material and to provide a significant source of energy for the dynamo. Similar to Si and O, we find a positive temperature dependence for Mg partitioning, but do not find as strong a pressure dependence. We also find a strong interaction with O in the metal, such that Mg is favored within the metallic phase as O in the metal increases. This result is different than initial studies of Mg partitioning (e.g., Badro et al., 2016; O'Rourke & Stevenson, 2016), but is similar to the results reported by Du et al. (2017) and Mittal et al. (2020). However,

despite the interaction with O, we find very low Mg concentrations in the cores of our model planets, in the range of 0.1–0.4 wt%. This is true regardless of whether Mg partitioning is treated as an exchange or dissociation reaction. It would require a substantial fraction of the core equilibration at very extreme temperatures, beyond the range of the experimental calibration of our metal-silicate parameterization, to reach the wt% levels of Mg in the core considered necessary in models of MgO exsolution (Badro et al., 2016; Mittal et al., 2020; O'Rourke & Stevenson, 2016). Further, those conditions would introduce a large amount of O into the core, which would serve to stabilize the Mg rather than driving it to precipitation. Thus, our results suggest that MgO precipitation was not a significant source of energy for the generation of the magnetic field.

Radioactive heat production could also play a role in the energy budget of the early core. Due to the scarcity of high temperature and pressure partitioning data, we cannot provide realistic estimates of the Th concentrations in the cores of our model planets (see Section 4.6). However, we are able to place constraints on the amount of K and U that could be partitioned into the core. Partitioning of K is too weak to have a significant influence on core dynamics. We find only a few parts per million of K partitions into the core, whereas the amount of K required to be an important heat source for the geodynamo exceeds several hundred ppm (Labrosse, 2015; Nimmo, 2015b). Our results fall to the lower end of previous estimates, which range from <1 ppm (Chabot & Drake, 1999), to a few tens of ppm (Blanchard et al., 2017; Bouhifd et al., 2007; Corgne, 2002; Hirao et al., 2006; Watanabe et al., 2014; Xiao & Stixrude, 2018). Some early studies suggested that high S content could result in several hundred ppm K in Earth's core (Gessmann & Wood, 2002; Murthy et al., 2003), but we find no dependence of K partitioning on the S content of the system. Note that the only radioactive isotope of K is ^{40}K, which makes up 0.012% of the total K abundance on Earth at present day, so most of the K partitioned into the core will not contribute to the heat budget.

On the other hand, all isotopes of U are radioactive and will contribute to the energy budget of the core, particularly ^{235}U early in Earth's history. We find that significant U can partition into the core at certain growth conditions. In our planetary growth calculations, we find several ppb U can be partitioned into the core with a strong positive dependence on the temperature of equilibration. These results are higher than early studies of U metal-silicate partitioning (<1 ppb Bouhifd et al., 2013; Malavergne et al., 2007), but are in line with more recent estimates (1–10 ppb Blanchard et al., 2017; Chidester et al., 2017; Wohlers & Wood, 2015). At our high end, 11 ppb U in the core would result in ∼4 TW of heat generated at 4.56 Ga. For context, thermal evolution models suggest that 200 ppm K, equivalent to ∼17 TW of heat released at 4.56 Ga, would be enough to solve the energy budget problem (Labrosse, 2015; Nimmo, 2015a). While this amount of U likely cannot solve the energy budget problem on its own, this amount of radiogenic heat could change the inferred initial temperature of the core by several hundred degrees, so must be accounted for in thermal evolution models.

6. Conclusions

We have experimentally determined metal-silicate partitioning of major, minor, and trace lithophile elements (Al, Ca, K, Mg, O, Si, Th, and U) and S to pressures of 85 GPa and temperatures up to 5400 K. Combining our data with literature data, we have devised a metal-silicate parameterization that accounts for pressure, temperature, and compositional dependencies in both the metal and silicate phases to predict the behavior of these elements over a wide range of conditions. We fit our parameterization for all terms and elements simultaneously to capture the complicated interactions between the partitioning of different elements. We find that such an approach is necessary to accurately determine the thermodynamic and chemical dependencies of partitioning. For example, increased temperatures favor partitioning of most lithophile elements into the metal, whether or not there is an explicit, non-compositional temperature dependence resolved. We also found that incorporating a silicate activity model into our parameterization significantly improved the fit for large cations, likely due to accommodation of large volume and/or charge for these elements within the silicate melt, and S, possibly due to changes in its valence state and mode of partitioning over the wide range of conditions covered by partitioning experiments.

We used our metal-silicate parameterization in a collection of planetary growth models to determine how different planetary accretion and core formation scenarios affected the composition of the mantle and core. The amount of S partitioned into the core in our models is small (<∼0.2 wt%), suggesting that the Earth's S depleted composition is the result of processes other than core formation. Although Si and O can both be partitioned into the core with abundances of up to several wt%, the other nominally lithophile elements in our study are present in much

smaller amounts. The modest amounts of Mg that are incorporated into the core in our models (<~0.4 wt%) and the positive pressure dependence we find for Si and O partitioning likely suggest that precipitation of oxides at the CMB is not a significant source of power for driving Earth's magnetic field unless a large fraction of the mass of the core underwent very high temperature equilibration. Such a scenario is probably unlikely, as much of the composition of the core is inherited from earlier stages of growth, limiting the effect of high temperature and pressure equilibration at the end of accretion. Conversely, we find that several ppb of U can be partitioned into the core, particularly at high temperatures, which should be accounted for in thermal evolution models of Earth's core.

We find that the FeO and SiO_2 contents of the mantle are very sensitive to the history of core formation, as well as the composition of the accreted material and, importantly, have opposite dependencies on the pressure and temperature of equilibration. Further, we find that Si partitioning into the core cannot account for observations of the mantle Mg/Si ratio; rather the bulk starting composition must be depleted in Si by about 8 wt% from the CI chondrite composition. Overall, our results support the conclusion that Earth's building blocks were relatively reduced and Fe-enriched, similar to enstatite chondrites (Dauphas et al., 2014). The abundances of moderately siderophile elements in the Earth's mantle have often been used to constrain the conditions of core formation (e.g., Fischer et al., 2015; Siebert et al., 2012), and our results suggest that the sensitivity of the mantle composition of major and nominally lithophile elements to the conditions of metal-silicate equilibration could provide powerful additional constraints on the accretional history of Earth.

Data Availability Statement

The data used in this study are provided in supplemental tables. These tables are available through the FAIR-compliant data repository Zenodo at https://doi.org/10.5281/zenodo.5722457.

Acknowledgments
The authors are grateful to Ingrid Blanchard and an anonymous reviewer for thoughtful comments on the manuscript. B. A. Chidester is grateful to Kellye Pando for help completing the piston-cylinder experiments and Minako Righter for completing the LA-ICP-MS measurements. This study was funded by an NSF Graduate Research Fellowship Grant # DGE-1144082 to B. A. Chidester and NSF Grant # EAR-1427123 to A. J. Campbell. B. A. Chidester was also funded by NASA Solar System Workings (# NNX15AH54G), the UC Office of the President Laboratory Fees Research Program (# LFR-17-449,059), and by the Department of Energy, National Nuclear Security Administration under Award Number DE-NA0003842. Support for K. Righter was provided by NASA's Planetary Science Research Program. S. J. Lock acknowledges funding from the Harvard Earth and Planetary Sciences Department, the Caltech Division of Geological and Planetary Sciences, NSF through awards EAR-1947614 and EAR-1725349, and UK NERC Grant NE/V014129/1.

References

Akahama, Y., & Kawamura, H. (2007). Diamond anvil Raman gauge in multimegabar pressure range. *High Pressure Research*, *27*(4), 473–482. https://doi.org/10.1080/08957950701659544

Anderson, O., & Isaak, D. (2002). Another look at the core density deficit of Earth's outer core. *Physics of the Earth and Planetary Interiors*, *131*(1), 19–27. https://doi.org/10.1016/S0031-9201(02)00017-1

Arevalo, R., McDonough, W. F., & Luong, M. (2009). The K/U ratio of the silicate Earth: Insights into mantle composition, structure and thermal evolution. *Earth and Planetary Science Letters*, *278*(3–4), 361–369. https://doi.org/10.1016/j.epsl.2008.12.023

Badro, J., Aubert, J., Hirose, K., Nomura, R., Blanchard, I., Borensztajn, S., & Siebert, J. (2018). Magnesium partitioning between Earth's mantle and core and its potential to drive an early exsolution geodynamo. *Geophysical Research Letters*, *45*(24), 213–240. https://doi.org/10.1029/2018GL080405

Badro, J., Côté, A. S., & Brodholt, J. P. (2014). A seismologically consistent compositional model of Earth's core. *Proceedings of the National Academy of Sciences of the United States of America*, *111*(21), 7542–7545. https://doi.org/10.1073/pnas.1316708111

Badro, J., Siebert, J., & Nimmo, F. (2016). An early geodynamo driven by exsolution of mantle components from Earth's core. *Nature*, *536*(7616), 326–328. https://doi.org/10.1038/nature18594

Ballhaus, C., Fonseca, R. O. C., Münker, C., Rohrbach, A., Nagel, T., Speelmanns, I. M., et al. (2017). The great sulfur depletion of Earth's mantle is not a signature of mantle–core equilibration. *Contributions to Mineralogy and Petrology*, *172*(8), 68. https://doi.org/10.1007/s00410-017-1388-3

Birch, F. (1952). Elasticity and constitution of the Earth's interior. *Journal of Geophysical Research*, *57*(2), 227–286. https://doi.org/10.1029/jz057i002p00227

Blanchard, I., Siebert, J., Borensztajn, S., & Badro, J. (2017). The solubility of heat-producing elements in Earth's core. *Geochemical Perspectives Letters*, *5*, 1–5. https://doi.org/10.7185/geochemlet.1737

Blundy, J., & Wood, B. (1994). Prediction of crystal-melt partition coefficients from elastic moduli. *Nature*, *372*(6505), 452–454. https://doi.org/10.1038/372452a0

Bouhifd, M. A., Andrault, D., Bolfan-Casanova, N., Hammouda, T., & Devidal, J. L. (2013). Metal-silicate partitioning of Pb and U: Effects of metal composition and oxygen fugacity. *Geochimica et Cosmochimica Acta*, *114*, 13–28. https://doi.org/10.1016/j.gca.2013.03.034

Bouhifd, M. A., Gautron, L., Bolfan-Casanova, N., Malavergne, V., Hammouda, T., Andrault, D., & Jephcoat, A. P. (2007). Potassium partitioning into molten iron alloys at high-pressure: Implications for Earth's core. *Physics of the Earth and Planetary Interiors*, *160*(1), 22–33. https://doi.org/10.1016/j.pepi.2006.08.005

Bouhifd, M. A., & Jephcoat, A. P. (2003). The effect of pressure on partitioning of Ni and Co between silicate and iron-rich metal liquids: A diamond-anvil cell study. *Earth and Planetary Science Letters*, *209*(1–2), 245–255. https://doi.org/10.1016/S0012-821X(03)00076-1

Bouhifd, M. A., & Jephcoat, A. P. (2011). Convergence of Ni and Co metal-silicate partition coefficients in the deep magma-ocean and coupled silicon-oxygen solubility in iron melts at high pressures. *Earth and Planetary Science Letters*, *307*, 341–348. https://doi.org/10.1016/j.epsl.2011.05.006

Boujibar, A., Andrault, D., Bouhifd, M. A., Bolfan-Casanova, N., Devidal, J. L., & Trcera, N. (2014). Metal-silicate partitioning of sulphur, new experimental and thermodynamic constraints on planetary accretion. *Earth and Planetary Science Letters*, *391*, 42–54. https://doi.org/10.1016/j.epsl.2014.01.021

Boujibar, A., Habermann, M., Righter, K., Ross, D. K., Pando, K., Righter, M., et al. (2019). U, Th, and K partitioning between metal, silicate, and sulfide and implications for Mercury's structure, volatile content, and radioactive heat production. *American Mineralogist*, *104*(9), 1221–1237. https://doi.org/10.2138/am-2019-7000

Boukaré, C.-E., Ricard, Y., & Fiquet, G. (2015). Thermodynamics of the MgO-FeO-SiO_2 system up to 140 GPa: Application to the crystallization of Earth's magma ocean. *Journal of Geophysical Research: Solid Earth*, *120*, 6085–6101. https://doi.org/10.1002/2015JB011929

Campbell, A. J. (2008). Measurement of temperature distributions across laser heated samples by multispectral imaging radiometry. *Review of Scientific Instruments*, *79*, 015108. https://doi.org/10.1063/1.2827513

Campbell, A. J., Seagle, C. T., Heinz, D. L., Shen, G., & Prakapenka, V. B. (2007). Partial melting in the iron-sulfur system at high pressure: A synchrotron X-ray diffraction study. *Physics of the Earth and Planetary Interiors*, *162*(1–2), 119–128. https://doi.org/10.1016/j.pepi.2007.04.001

Canup, R. M. (2012). Composition via a giant impact. *Science*, *338*, 1052–1055. https://doi.org/10.1126/science.1226073

Canup, R. M., & Ashpaug, E. (2001). Origin of the Moon in a giant impact near the end of the Earth's formation. *Nature*, *412*(6848), 708–712. https://doi.org/10.1038/35089010

Carter, P. J., Lock, S. J., & Stewart, S. T. (2020). The energy budgets of giant impacts. *Journal of Geophysical Research: Planets*, *125*, e2019JE006042. https://doi.org/10.1029/2019JE006042

Chabot, N. L., & Drake, M. J. (1999). Potassium solubility in metal: The effects of composition at 15 kbar and 1900°C on partitioning between iron alloys and silicate melts. *Earth and Planetary Science Letters*, *172*(3–4), 323–335. https://doi.org/10.1016/S0012-821X(99)00208-3

Chidester, B. A., Rahman, Z., Righter, K., & Campbell, A. J. (2017). Metal–silicate partitioning of U: Implications for the heat budget of the core and evidence for reduced U in the mantle. *Geochimica et Cosmochimica Acta*, *199*, 1–12. https://doi.org/10.1016/j.gca.2016.11.035

Corgne, A., Allan, N. L., & Wood, B. J. (2003). Atomistic simulations of trace element incorporation into the large site of $MgSiO_3$ and $CaSiO_3$ perovskites. *Physics of the Earth and Planetary Interiors*, *139*(1–2), 113–127. https://doi.org/10.1016/S0031-9201(03)00148-1

Corgne, A., Keshav, S., Fei, Y., & McDonough, W. F. (2007). How much potassium is in the Earth's core? New insights from partitioning experiments. *Earth and Planetary Science Letters*, *256*(3–4), 567–576. https://doi.org/10.1016/j.epsl.2007.02.012

Corgne, A., Liebske, C., Wood, B. J., Rubie, D. C., & Frost, D. J. (2005). Silicate perovskite-melt partitioning of trace elements and geochemical signature of a deep perovskitic reservoir. *Geochimica et Cosmochimica Acta*, *69*(2), 485–496. https://doi.org/10.1016/j.gca.2004.06.041

Corgne, A., & Wood, B. J. (2002). $CaSiO_3$ and $CaTiO_3$ perovskite-melt partitioning of trace elements: Implications for gross mantle differentiation. *Geophysical Research Letters*, *29*(19), 3–1. https://doi.org/10.1029/2001GL014398

Cuk, M., & Stewart, S. T. (2012). Making the moon from a fast-spinning by resonant despinning. *Science*, *338*(6110), 1047–1052. https://doi.org/10.1126/science.1225542

Dauphas, N., Chen, J. H., Zhang, J., Papanastassiou, D. A., Davis, A. M., & Travaglio, C. (2014). Calcium-48 isotopic anomalies in bulk chondrites and achondrites: Evidence for a uniform isotopic reservoir in the inner protoplanetary disk. *Earth and Planetary Science Letters*, *407*, 96–108. https://doi.org/10.1016/j.epsl.2014.09.015

Dauphas, N., Poitrasson, F., Burkhardt, C., Kobayashi, H., & Kurosawa, K. (2015). Planetary and meteoritic Mg/Si and delta-30Si variations inherited from solar nebula chemistry. *Earth and Planetary Science Letters*, *427*, 236–248. https://doi.org/10.1016/j.epsl.2015.07.008

de Koker, N., Steinle-Neumann, G., & Vlcek, V. (2012). Electrical resistivity and thermal conductivity of liquid Fe alloys at high P and T, and heat flux in Earth's core. *Proceedings of the National Academy of Sciences of the United States of America*, *109*(11), 4070–4073. https://doi.org/10.1073/pnas.1111841109

Du, Z., Jackson, C., Bennett, N., Driscoll, P., Deng, J., Lee, K. K. M., et al. (2017). Insufficient energy from MgO exsolution to power early geodynamo. *Geophysical Research Letters*, *44*(22), 376–411. https://doi.org/10.1002/2017GL075283

Dziewonski, A. M., & Anderson, D. L. (1981). Preliminary reference Earth model. *Physics of the Earth and Planetary Interiors*, *25*(4), 297–356. https://doi.org/10.1016/0031-9201(81)90046-7

Faure, P., Bouhifd, M. A., Boyet, M., Manthilake, G., Clesi, V., & Devidal, J. L. (2020). Uranium and thorium partitioning in the bulk silicate Earth and the oxygen content of Earth's core. *Geochimica et Cosmochimica Acta*, *275*, 83–98. https://doi.org/10.1016/j.gca.2020.02.010

Filiberto, J., Treiman, A. H., & Le, L. (2008). Crystallization experiments on a Gusev Adirondack basalt composition. *Meteoritics & Planetary Science*, *43*(7), 1137–1146. https://doi.org/10.1111/j.1945-5100.2008.tb01118.x

Fiquet, G., Auzende, A. L., Siebert, J., Corgne, A., Bureau, H., Ozawa, H., & Garbarino, G. (2010). Melting of peridotite to 140 gigapascals. *Science*, *329*(5998), 1516–1518. https://doi.org/10.1126/science.1192448

Fischer, R. A., Campbell, A. J., Chidester, B. A., Reaman, D. M., Thompson, E. C., Pigott, J. S., et al. (2018). Equations of state and phase boundary for stishovite and $CaCl_2$-type SiO_2. *American Mineralogist*, *103*(5), 792–802. https://doi.org/10.2138/am-2018-6267

Fischer, R. A., Campbell, A. J., & Ciesla, F. J. (2017). Sensitivities of Earth's core and mantle compositions to accretion and differentiation processes. *Earth and Planetary Science Letters*, *456*, 252–262. https://doi.org/10.1016/j.epsl.2016.10.025

Fischer, R. A., Nakajima, Y., Campbell, A. J., Frost, D. J., Harries, D., Langenhorst, F., et al. (2015). High pressure metal–silicate partitioning of Ni, Co, V, Cr, Si, and O. *Geochimica et Cosmochimica Acta*, *167*, 177–194. https://doi.org/10.1016/j.gca.2015.06.026

Gessmann, C. K., & Wood, B. J. (2002). Potassium in the Earth's core? *Earth and Planetary Science Letters*, *200*, 63–78. https://doi.org/10.1016/s0012-821x(02)00593-9

Goldstein, J. I., Scott, E. R. D., & Chabot, N. L. (2009). Iron meteorites: Crystallization, thermal history, parent bodies, and origin. *Geochemistry*, *69*(4), 293–325. https://doi.org/10.1016/j.chemer.2009.01.002

Heinz, D. L., & Jeanloz, R. (1987). Temperature measurements in the laser-heated diamond cell. In M. H. Manhnani & Y. Syono (Eds.), *High-pressure research in mineral physics* (pp. 113–127). American Geophysical Union. https://doi.org/10.1029/gm039p0113

Hirao, N., Ohtani, E., Kondo, T., Endo, N., Kuba, T., Suzuki, T., & Kikegawa, T. (2006). Partitioning of potassium between iron and silicate at the core-mantle boundary. *Geophysical Research Letters*, *33*(8), 33–36. https://doi.org/10.1029/2005GL025324

Hirose, K., Morard, G., Sinmyo, R., Umemoto, K., Hernlund, J., Helffrich, G., & Labrosse, S. (2017). Crystallization of silicon dioxide and compositional evolution of the Earth's core. *Nature*, *543*(7643), 99–102. https://doi.org/10.1038/nature21367

Holzheid, A., Palme, H., & Chakraborty, S. (1997). The activities of NiO, CoO and FeO in silicate melts. *Chemical Geology*, *139*(1–4), 21–38. https://doi.org/10.1016/S0009-2541(97)00030-2

Ito, E., Kubo, A., Katsura, T., & Walter, M. J. (2004). Melting experiments of mantle materials under lower mantle conditions with implications for magma ocean differentiation. *Physics of the Earth and Planetary Interiors*, *143*(1–2), 397–406. https://doi.org/10.1016/j.pepi.2003.09.016

Jackson, C. R. M., Bennett, N. R., Du, Z., Cottrell, E., & Fei, Y. (2018). Early episodes of high-pressure core formation preserved in plume mantle. *Nature*, *553*(7689), 491–495. https://doi.org/10.1038/nature25446

Japan Society for the Advancement of Science and the 19th Committee on Steelmaking. (1988). *Steelmaking data sourcebook* (revised ed.). Gordon and Breach Science Publishers.

Jennings, E. S., Wade, J., Laurenz, V., & Petitgirard, S. (2019). Diamond anvil cell partitioning experiments for accretion and core formation: Testing the limitations of electron microprobe analysis. *Microscopy and Microanalysis*, *25*(1), 1–10. https://doi.org/10.1017/S1431927618015568

Kendall, J. D., & Melosh, H. J. (2016). Differentiated planetesimal impacts into a terrestrial magma ocean: Fate of the iron core. *Earth and Planetary Science Letters*, *448*, 24–33. https://doi.org/10.1016/j.epsl.2016.05.012

Labrosse, S. (2015). Thermal evolution of the core with a high thermal conductivity. *Physics of the Earth and Planetary Interiors*, *247*, 36–55. https://doi.org/10.1016/j.pepi.2015.02.002

Lacaze, J., & Sundman, B. (1991). An assessment of the Fe-C-Si system. *Metallurgical Transactions A*, *22*(10), 2211–2223. https://doi.org/10.1007/BF02664987

Landeau, M., Olson, P., Deguen, R., & Hirsh, B. H. (2016). Core merging and stratification following giant impact. *Nature Geoscience*, *9*(10), 786–789. https://doi.org/10.1038/ngeo2808

Laurenz, V., Rubie, D. C., Frost, D. J., & Vogel, A. K. (2016). The importance of sulfur for the behavior of highly-siderophile elements during Earth's differentiation. *Geochimica et Cosmochimica Acta*, *194*, 123–138. https://doi.org/10.1016/j.gca.2016.08.012

Lherm, V., & Deguen, R. (2018). Small-scale metal/silicate equilibration during core formation: The influence of stretching enhanced diffusion on mixing. *Journal of Geophysical Research: Solid Earth*, *123*(12), 496–510. https://doi.org/10.1029/2018JB016537

Lock, S. J., & Stewart, S. T. (2017). The structure of terrestrial bodies: Impact heating, corotation limits, and synestias. *Journal of Geophysical Research: Planets*, *122*, 950–982. https://doi.org/10.1002/2016JE005239

Lock, S. J., & Stewart, S. T. (2019). Giant impacts stochastically change the internal pressures of terrestrial planets. *Science Advances*, *5*(9), eaav3746. https://doi.org/10.1126/sciadv.aav3746

Lodders, K. (2003). Solar system Abundances and condensation temperatures of the elements. *The Astrophysical Journal*, *591*(2), 1220–1247. https://doi.org/10.1086/375492

Ma, Z. (2001). Thermodynamic description for concentrated metallic solutions using interaction parameters. *Metallurgical and Materials Transactions B*, *32*(1), 87–103. https://doi.org/10.1007/s11663-001-0011-0

Mahan, B., Siebert, J., Blanchard, I., Badro, J., Kubik, E., Sossi, P., & Moynier, F. (2018). Investigating Earth's formation history through copper and sulfur metal-silicate partitioning during core-mantle differentiation. *Journal of Geophysical Research: Solid Earth*, *123*, 8349–8363. https://doi.org/10.1029/2018JB015991

Malavergne, V., Tarrida, M., Combes, R., Bureau, H., Jones, J., & Schwandt, C. (2007). New high-pressure and high-temperature metal/silicate partitioning of U and Pb: Implications for the cores of the Earth and Mars. *Geochimica et Cosmochimica Acta*, *71*, 2637–2655. https://doi.org/10.1016/j.gca.2007.03.011

McDonough, W. F., & Sun, S. s. (1995). The composition of the Earth. *Chemical Geology*, *120*(3–4), 223–253. https://doi.org/10.1016/0009-2541(94)00140-4

Mittal, T., Knezek, N., Arveson, S. M., McGuire, C. P., Williams, C. D., Jones, T. D., & Li, J. (2020). Precipitation of multiple light elements to power Earth's early dynamo. *Earth and Planetary Science Letters*, *532*, 116030. https://doi.org/10.1016/j.epsl.2019.116030

Miyazaki, Y., & Korenaga, J. (2019). On the timescale of magma ocean solidification and its chemical consequences: 1. Thermodynamic database for liquid at high pressures. *Journal of Geophysical Research B: Solid Earth*, *124*(4), 3382–3398. https://doi.org/10.1029/2018jb016932

Mukhopadhyay, B., Basu, S., & Holdaway, M. J. (1993). A discussion of Margules-type formulations for multicomponent solutions with a generalized approach. *Geochimica et Cosmochimica Acta*, *57*(2), 277–283. https://doi.org/10.1016/0016-7037(93)90430-5

Murthy, V. R., van Westrenen, W., & Fei, Y. (2003). Experimental evidence that potassium is a substantial radioactive heat source in planetary cores. *Nature*, *423*(6936), 163–165. https://doi.org/10.1038/nature01560

Nimmo, F. (2015a). Energetics of the core. In *Treatise on geophysics* (2nd ed., Vol. 8, pp. 31–65). Elsevier BV. https://doi.org/10.1016/B978-044452748-6.00128-0

Nimmo, F. (2015b). Thermal and compositional evolution of the core. In G. Shubert (Ed.), *Treatise on geophysics* (2nd ed., Vol. 9, pp. 201–219). Elsevier BV. https://doi.org/10.1016/b978-0-444-53802-4.00160-3

Nimmo, F., Price, G. D., Brodholt, J., & Gubbins, D. (2004). The influence of potassium on core and geodynamo evolution. *Geophysical Journal International*, *156*(2), 363–376. https://doi.org/10.1111/j.1365-246X.2003.02157.x

O'Neill, H. S. C. (1991). The origin of the Moon and the early history of the Earth – A chemical model. Part 2: The Earth. *Geochimica et Cosmochimica Acta*, *55*, 1159–1172. https://doi.org/10.1016/0016-7037(91)90168-5

O'Neill, H. S. C., & Eggins, S. M. (2002). The effect of melt composition on trace element partitioning: An experimental investigation of the activity coefficients of FeO, NiO, CoO, MoO_2 and MoO_3 in silicate melts. *Chemical Geology*, *186*(1–2), 151–181. https://doi.org/10.1016/S0009-2541(01)00414-4

O'Rourke, J. G., Korenaga, J., & Stevenson, D. J. (2017). Thermal evolution of Earth with magnesium precipitation in the core. *Earth and Planetary Science Letters*, *458*, 263–272. https://doi.org/10.1016/j.epsl.2016.10.057

O'Rourke, J. G., & Stevenson, D. J. (2016). Powering Earth's dynamo with magnesium precipitation from the core. *Nature*, *529*, 387–389. https://doi.org/10.1038/nature16495

Palme, H., & O'Neill, H. (2013). Cosmochemical estimates of mantle composition. *Treatise on Geochemistry* (2nd ed., Vol. 3, pp. 1–39). https://doi.org/10.1016/B978-0-08-095975-7.00201-1

Pearce, N. J. G., Perkins, W. T., Westgate, J. A., Gorton, M. P., Jackson, S. E., Neal, C. R., & Chenery, S. P. (1997). A compilation of new and published major and trace element data for NIST SRM 610 and NIST SRM 612 glass reference materials. *Geostandards and Geoanalytical Research*, *21*(1), 115–144. https://doi.org/10.1111/j.1751-908x.1997.tb00538.x

Piet, H., Badro, J., & Gillet, P. (2017). Geochemical constraints on the size of the moon-forming giant impact. *Geophysical Research Letters*, *44*(23), 711–11. https://doi.org/10.1002/2017GL075225

Pozzo, M., Davies, C., Gubbins, D., & Alfè, D. (2012). Thermal and electrical conductivity of iron at Earth's core conditions. *Nature*, *485*, 355–358. https://doi.org/10.1038/nature11031

Righter, K. (2002). Does the moon have a metallic core? Constraints from giant impact modeling and siderophile elements. *Icarus*, *158*(1), 1–13. https://doi.org/10.1006/icar.2002.6859

Righter, K., Pando, K., Humayun, M., Waeselmann, N., Yang, S., Boujibar, A., & Danielson, L. R. (2018). Effect of silicon on activity coefficients of siderophile elements (Au, Pd, Pt, P, Ga, Cu, Zn, and Pb) in liquid Fe: Roles of core formation, late sulfide matte, and late veneer in shaping terrestrial mantle geochemistry. *Geochimica et Cosmochimica Acta*, *232*, 101–123. https://doi.org/10.1016/j.gca.2018.04.011

Righter, K., Pando, K. M., Danielson, L., & Lee, C. T. (2010). Partitioning of Mo, P and other siderophile elements (Cu, Ga, Sn, Ni, Co, Cr, Mn, V, and W) between metal and silicate melt as a function of temperature and silicate melt composition. *Earth and Planetary Science Letters*, *291*(1–4), 1–9. https://doi.org/10.1016/j.epsl.2009.12.018

Righter, K., Schönbächler, M., Pando, K., Rowland, R., Righter, M., & Lapen, T. (2020). Ag isotopic and chalcophile element evolution of the terrestrial and martian mantles during accretion: New constraints from Bi and Ag metal-silicate partitioning. *Earth and Planetary Science Letters*, *552*, 116590. https://doi.org/10.1016/j.epsl.2020.116590

Righter, K., Sutton, S. R., Newville, M., Le, L., Schwandt, C. S., Uchida, H., et al. (2006). An experimental study of the oxidation state of vanadium in spinel and basaltic melt with implications for the origin of planetary basalt. *American Mineralogist*, *91*, 1643–1656. https://doi.org/10.2138/am.2006.2111

Rubie, D. C., Frost, D. J., Mann, U., Asahara, Y., Nimmo, F., Tsuno, K., et al. (2011). Heterogeneous accretion, composition and core-mantle differentiation of the Earth. *Earth and Planetary Science Letters*, *301*, 31–42. https://doi.org/10.1016/j.epsl.2010.11.030

Rubie, D. C., Jacobson, S. A., Morbidelli, A., O'Brien, D. P., Young, E. D., de Vries, J., et al. (2015). Accretion and differentiation of the terrestrial planets with implications for the compositions of early-formed Solar System bodies and accretion of water. *Icarus*, *248*, 89–108. https://doi.org/10.1016/j.icarus.2014.10.015

Rubie, D. C., Laurenz, V., Jacobson, S. A., Morbidelli, A., Palme, H., Vogel, A. K., & Frost, D. J. (2016). Highly siderophile elements were stripped from Earth's mantle by iron sulfide segregation. *Science*, *353*(6304), 1141–1144. https://doi.org/10.1126/science.aaf6919

Rubie, D. C., Nimmo, F., & Melosh, H. J. (2015). *Formation of the Earth's core* (Vol. 9, pp. 43–79). Elsevier BV. https://doi.org/10.1016/B978-0-444-53802-4.00154-8

Rudge, J. F., Kleine, T., & Bourdon, B. (2010). Broad bounds on Earths accretion and core formation constrained by geochemical models. *Nature Geoscience*, *3*(6), 439–443. https://doi.org/10.1038/ngeo872

Schrader, D. L., Lauretta, D. S., Connolly, H. C., Goreva, Y. S., Hill, D. H., Domanik, K. J., et al. (2010). Sulfide-rich metallic impact melts from chondritic parent bodies. *Meteoritics and Planetary Science*, *45*(5), 743–758. https://doi.org/10.1111/j.1945-5100.2010.01053.x

Shearer, P., & Masters, G. (1990). The density and shear velocity contrast at the inner core boundary. *Geophysical Journal International*, *102*, 491–498. https://doi.org/10.1111/j.1365-246X.1990.tb04481.x

Siebert, J., Badro, J., Antonangeli, D., & Ryerson, F. J. (2012). Metal-silicate partitioning of Ni and Co in a deep magma ocean. *Earth and Planetary Science Letters*, *321–322*, 189–197. https://doi.org/10.1016/j.epsl.2012.01.013

Siebert, J., Corgne, A., & Ryerson, F. J. (2011). Systematics of metal–silicate partitioning for many siderophile elements applied to Earth's core formation. *Geochimica et Cosmochimica Acta*, *75*(6), 1451–1489. https://doi.org/10.1016/j.gca.2010.12.013

Siebert, J., Sossi, P. A., Blanchard, I., Mahan, B., Badro, J., & Moynier, F. (2018). Chondritic Mn/Na ratio and limited post-nebular volatile loss of the Earth. *Earth and Planetary Science Letters*, *485*, 130–139. https://doi.org/10.1016/j.epsl.2017.12.042

Stebbins, J. F., Carmichael, I. S. E., & Moret, L. K. (1984). Heat capacities and entropies of silicate liquids and glasses. *Contributions to Mineralogy and Petrology*, *86*(2), 131–148. https://doi.org/10.1007/BF00381840

Stewart, S. T., Davies, E. J., Duncan, M., Lock, S., Root, S., Townsend, J. P., et al. (2020). The shock physics of giant impacts: Key requirements for the equations of state. In *AIP conference proceedings* (Vol. 2272, p. 080003). AIP Publishing LLC. https://doi.org/10.1063/12.0000946

Suer, T. A., Siebert, J., Remusat, L., Menguy, N., & Fiquet, G. (2017). A sulfur-poor terrestrial core inferred from metal–silicate partitioning experiments. *Earth and Planetary Science Letters*, *469*, 84–97. https://doi.org/10.1016/j.epsl.2017.04.016

Tarduno, J. A., Cottrell, R. D., Davis, W. J., Nimmo, F., & Bono, R. K. (2015). A Hadean to Paleoarchean geodynamo recorded by single zircon crystals. *Science*, *349*(6247), 521–524. https://doi.org/10.1126/science.aaa9114

Tarduno, J. A., Cottrell, R. D., Watkeys, M. K., Hofmann, A., Doubrovine, P. V., Mamajek, E. E., et al. (2010). Geodynamo, solar wind, and magnetopause 3.4 to 3.45 billion years ago. *Science*, *327*(5970), 1238–1240. https://doi.org/10.1126/science.1183445

Trønnes, R. G., Baron, M. A., Eigenmann, K. R., Guren, M. G., Heyn, B. H., Løken, A., & Mohn, C. E. (2019). Core formation, mantle differentiation and core-mantle interaction within Earth and the terrestrial planets. *Tectonophysics*, *760*, 165–198. https://doi.org/10.1016/j.tecto.2018.10.021

van Achterbergh, E., Ryan, C. G., & Griffin, W. L. (1999). GLITTER: Online interactive data reduction for the laser ablation inductively coupled plasma mass spectrometery microprobe. *Proceedings of the 9th V. M. Goldschmidt Conference* (pp. 305–306).

Vander Kaaden, K. E., McCubbin, F. M., Turner, A. A., & Ross, D. K. (2020). Constraints on the abundances of carbon and silicon in Mercury's core from experiments in the Fe-Si-C system. *Journal of Geophysical Research: Planets*, *125*(5), 1–15. https://doi.org/10.1029/2019JE006239

Wade, J., & Wood, B. (2005). Core formation and the oxidation state of the Earth. *Earth and Planetary Science Letters*, *236*(1–2), 78–95. https://doi.org/10.1016/j.epsl.2005.05.017

Wade, J., & Wood, B. J. (2001). The Earth's 'missing' niobium may be in the core. *Nature*, *409*(6816), 75–78. https://doi.org/10.1038/35051064

Watanabe, K., Ohtani, E., Kamada, S., Sakamaki, T., Miyahara, M., & Ito, Y. (2014). The abundance of potassium in the Earth's core. *Physics of the Earth and Planetary Interiors*, *237*, 65–72. https://doi.org/10.1016/j.pepi.2014.10.001

Wohlers, A., & Wood, B. J. (2015). A Mercury-like component of early Earth yields uranium in the core and high mantle 142Nd. *Nature*, *520*(7547), 337–340. https://doi.org/10.1038/nature14350

Wohlers, A., & Wood, B. J. (2017). Uranium, thorium and REE partitioning into sulfide liquids: Implications for reduced S-rich bodies. *Geochimica et Cosmochimica Acta*, *205*, 226–244. https://doi.org/10.1016/j.gca.2017.01.050

Wood, B. J., Kiseeva, E. S., & Mirolo, F. J. (2014). Accretion and core formation: The effects of sulfur on metal-silicate partition coefficients. *Geochimica et Cosmochimica Acta*, *145*, 248–267. https://doi.org/10.1016/j.gca.2014.09.002

Xiao, B., & Stixrude, L. (2018). Critical vaporization of $MgSiO_3$. *Proceedings of the National Academy of Sciences of the United States of America*, *115*(21), 5371–5376. https://doi.org/10.1073/pnas.1719134115